

An Observational Study of Mesoscale Convective Systems with Heavy Rainfall over the Korean Peninsula

HYUNG WOO KIM AND DONG KYOU LEE

Atmospheric Sciences Program, School of Earth and Environmental Sciences, Seoul National University, Seoul, South Korea

(Manuscript received 11 August 2004, in final form 7 September 2005)

ABSTRACT

A heavy rainfall event induced by mesoscale convective systems (MCSs) occurred over the middle Korean Peninsula from 25 to 27 July 1996. This heavy rainfall caused a large loss of life and property damage as a result of flash floods and landslides. An observational study was conducted using Weather Surveillance Radar-1988 Doppler (WSR-88D) data from 0930 UTC 26 July to 0303 UTC 27 July 1996. Dominant synoptic features in this case had many similarities to those in previous studies, such as the presence of a quasi-stationary frontal system, a weak upper-level trough, sufficient moisture transportation by a low-level jet from a tropical storm landfall, strong potential and convective instability, and strong vertical wind shear. The thermodynamic characteristics and wind shear presented favorable conditions for a heavy rainfall occurrence. The early convective cells in the MCSs initiated over the coastal area, facilitated by the mesoscale boundaries of the land-sea contrast, rain-no rain regions, saturated-unsaturated soils, and steep horizontal pressure and thermal gradients. Two MCSs passed through the heavy rainfall regions during the investigation period. The first MCS initiated at 1000 UTC 26 July and had the characteristics of a supercell storm with small amounts of precipitation, the appearance of a mesocyclone with tilting storm, a rear-inflow jet at the midlevel of the storm, and fast forward propagation. The second MCS initiated over the upstream area of the first MCS at 1800 UTC 26 July and had the characteristics of a multicell storm, such as a broken areal-type squall line, slow or quasi-stationary backward propagation, heavy rainfall in a concentrated area due to the merging of the convective storms, and a stagnated cluster system. These systems merged and stagnated because their movement was blocked by the Taebaek Mountain Range, and they continued to develop because of the vertical wind shear resulting from a low-level easterly inflow.

1. Introduction

Heavy rainfall during the summer season is one of the most significant factors in natural disasters on the Korean Peninsula. Most heavy rainfall events are related to mesoscale convective systems (MCSs; Zipser 1982), which occur under certain synoptic-scale environmental conditions, such as a surface frontal system accompanying an upper-level trough during the changma (mei-yu in China, baiu in Japan) period, or strong instability in the vicinity of the subtropical Pacific high in the postchangma period (Lee et al. 1998). Under the latter condition, it is difficult to distinguish

indicators of MCS outbreaks from synoptic-scale observations due to their small spatial and temporal scales. According to previous studies (Lee et al. 1998; Sun and Lee 2002), favorable conditions for heavy rainfall in Korea are as follows: a southwesterly low-level jet stream (LLJ), cold-air advection associated with upper-level disturbances, potential instability, a warm moisture tongue and warm advection originating from southern and central China, and an intensified upper-level jet stream with strong baroclinicity. Moreover, numerical simulation studies show that the dynamic and physical process of heavy rainfall over Korea can be identified and MCSs accompanying heavy rainfall are, to a certain extent, predictable (Wee 1999; Sun and Lee 2002).

Even though the most favorable synoptic conditions for heavy rainfall are found from synoptic-scale observations and numerical model results, it remains a great challenge for operational forecasters to identify the lo-

Corresponding author address: Dong Kyou Lee, Atmospheric Science Program, School of Earth and Environmental Sciences, Seoul National University, Sinrimdong, Kwanakgu, Seoul 151-742, South Korea.
E-mail: dklee@snu.ac.kr

cation and time of MCS onset, to predict the evolution and movement of the storms, and the mechanisms leading to heavy rainfall. In studies of kinematic and dynamic structures of MCSs since the 1970s, Doppler radar imagery has played an increasingly important role (Burgess and Ray 1986). Bluestein and Jain (1985) investigated MCSs in the midlatitudes and suggested the existence a type of precipitation band, referred to as a squall line, using radar imagery. Houze et al. (1989) demonstrated a conceptual model of MCS structure, in which the precipitation structures of MCSs are composed of convective precipitation areas, transition zones, and trailing stratiform precipitation areas. It is generally accepted that the spatially and temporally high-resolution data from Weather Surveillance Radars-1988 Doppler (WSR-88D) has led to significant improvement in short-range forecasts and warnings for severe convective storms and flash floods in the United States (Serafin and Wilson 2000). MCSs or mesoscale convective complexes are considered to be primary factors for severe weather events, such as high winds, hail, and heavy rainfall around the world. Heavy rainfall related to MCSs is very common in east Asia during the summer, especially the summer monsoon period.

There have been many studies of heavy rainfall and cloud physics using Doppler radar findings since the 1980s. Takeda and Takase (1980) showed that a long-lasting precipitation system was maintained as a group of small precipitating convective clouds forming successively in the same area. Watanabe and Ogura (1987) showed that convective cells formed in succession about 50 km off the coast during a heavy precipitation period under very moist conditions up to 600 hPa. Recently, field observations have provided useful information on meso- α - and meso- β scale structures and their development in monsoon frontal systems from Doppler radar observations (Moteki et al. 2004a,b). In Korea, Chun and Oh (1991) retrieved the horizontal wind field from a single Doppler radar image and showed that the maximum convergence occurred prior to the maximum rainfall intensity, and that the maximum convergence and rainfall intensity zone coincided. However, an observational study on heavy rainfall events accompanying MCSs using volume-scanned Doppler radar data had not yet been conducted in Korea. Now, mesoscale observational features of heavy rainfall events are provided by the United States Air Force's WSR-88D at the Pyongtaek Air Base in Korea.

The purpose of this paper is to investigate the initiation and evolution of convective storms embedded in MCSs, the movement and propagation of storms, and the structure and kinematics of convective storms for

the heavy rainfall that occurred in the middle of the Korean Peninsula from 26 to 27 July 1996 using synoptic-scale and WSR-88D data.

2. Data and methodology

Data used in this study were taken from Japan Meteorological Agency analysis charts, the National Centers for Environmental and Prediction–National Center for Atmospheric Research (NCEP–NCAR) reanalysis dataset of the horizontal resolution at $2.5^\circ \times 2.5^\circ$ and 12 vertical layers, Korea Meteorological Administration (KMA) and Republic of Korea Air Force (ROKAF) surface observations, and the *Geostationary Meteorological Satellite-5 (GMS-5)* with 3-h intervals and imagery of 1-h intervals. Rawinsonde (raob) data of 6-h intervals at the Osan ROKAF station and the 1-h interval precipitation data from KMA and ROKAF were also used. The main mesoscale data were WSR-88D level II data, which have 14 elevation levels with about 5-min intervals. The area of cloud-top temperature less than -32°C was selected to trace MCS movement and to identify the strong convective region. The raob data from the Osan weather station were analyzed by the complete Rawinsonde Observation Program, version 5.5 (RAOB55; ERS 2004). The RAOB55 allowed both analysis of skew T and the hodograph chart and also calculation of thermodynamic indices and wind data, which helped to infer convective potential, storm type, and movement. The Doppler radar data were analyzed and visualized using the WSR-88D Algorithm Testing and Display System, version 10.0 (WATADS 10.0; SSAD 1998), developed at the National Severe Storm Laboratory (NSSL) and the Radar Operations Center (ROC). The WATADS system utilizes special meteorological algorithms to process and analyze data in order to detect and analyze severe weather events (Johnson et al. 1998). WATADS displays reflectivity, radial velocity, and spectrum width as colorized imagery and alphanumeric values for selected points.

3. The heavy rainfall events at Chorwon and Yonchon

a. Brief case description

From 25 to 27 July 1996, heavy rainfall resulting from MCSs occurred over the central Korean Peninsula. The heavy rainfall produced devastating flash floods and landslides, causing 86 fatalities and about \$480 million (U.S.) in property damage. In general, the Korean Peninsula is dominated by hot, humid, and generally sultry

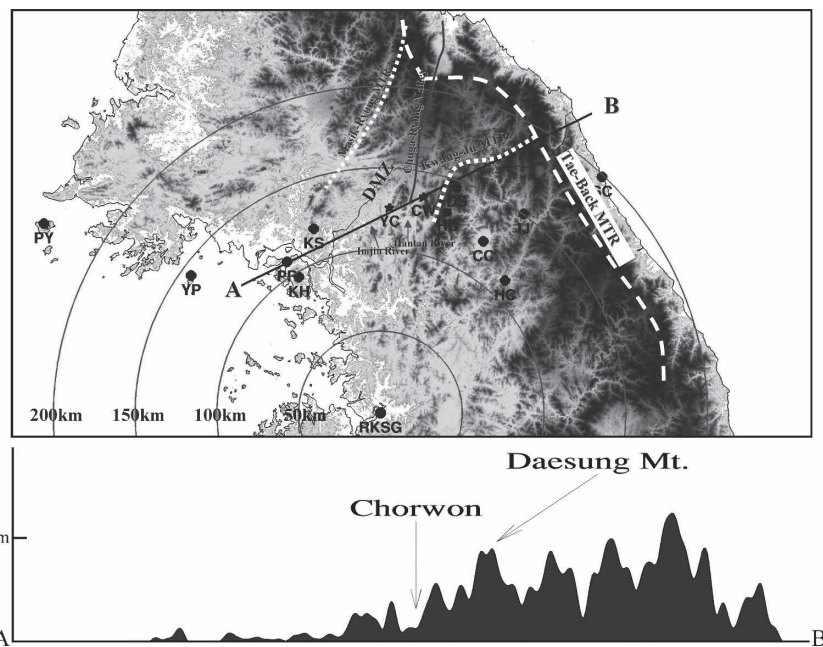


FIG. 1. (a) Topographical and geographical distribution over the central Korean Peninsula (top) and (b) cross section of topography along the line A–B. Also, refer to Fig. 3 for the location of the central Korean Peninsula.

weather after the changma period, from the end of July through the middle of August. However, abnormal and strong heavy rainfalls causing tremendous damage sometimes occur over the Korean Peninsula after the changma period, as was the case in July 1996 (KMA 1996).

The successive rainfall events started in the western coastal region of the northern Korean Peninsula on 25 July and moved gradually southeastward along the coast. Then, they were almost stationary in the mid-western Korean Peninsula from 26 to 27 July 1996, during which a number of deep convective storms responsible for heavy rainfall were initiated over the coastal area of the midwestern Korean Peninsula near the Demilitarized Zone (DMZ), which separates North and South Korea. The rainfall amounts at the Chorwon station exceeded 250 mm for 24 h. The synoptic-scale and mesoscale observational data were not sufficient for an operational prediction and research analysis, because the heavy rain region was located near the DMZ and in North Korea. As mentioned above, one of the important observational datasets available for the analysis of this case was from the WSR-88D.

b. Topography of the mid-Korean Peninsula

Figure 1 illustrates the topography of the mid-Korean Peninsula with coverage range of the WSR-88D (RKSG) with a 50-km interval. KMA and

ROKAF weather stations at Paengnyungdo (PY), Yeonpyeungdo (YP), Pyoripsan (PR), Kanghwado (KH), Yonchon (YC), Chorwon (CW), Daesungsan (DS), Hwachon (HC), Chunchon (CC), Hongchon (HC), Inje (IJ), and Sockcho (SC) are designated. The Taebaek Mountain (TBM) Range with elevations over 1.5 km runs from north to south and serves as the backbone of the Korean Peninsula. The Masikryung and Kwangju Mountain Ranges, with about 100 km between them, extend from the TBM Range toward the Yellow Sea (from east to west) and the Chugaryung Valley lies between these two ranges. The Imjin River, the Hantan River, and about 20 small streams flow along the Chugaryung Valley area, and the plain field is well developed around the river basins with elevations of 200 ~ 300 m. Chorwon and Yonchon are located in this relatively low-elevation region with the Kwangju Mountain Range in the background. The eastern and southeastern sides of Chorwon and Yonchon are surrounded by mountains, while their western and northwestern sides are exposed. The topographical distributions of water bodies, vegetation cover, and soil type are considered to be important mechanisms that influence the formation of severe convective storms (Doswell 2001). When sufficient moisture is present, the complex terrain often supports vigorous convective activities. According to Watanabe and Ogura (1987), favorable regions for the occurrence of heavy rainfall

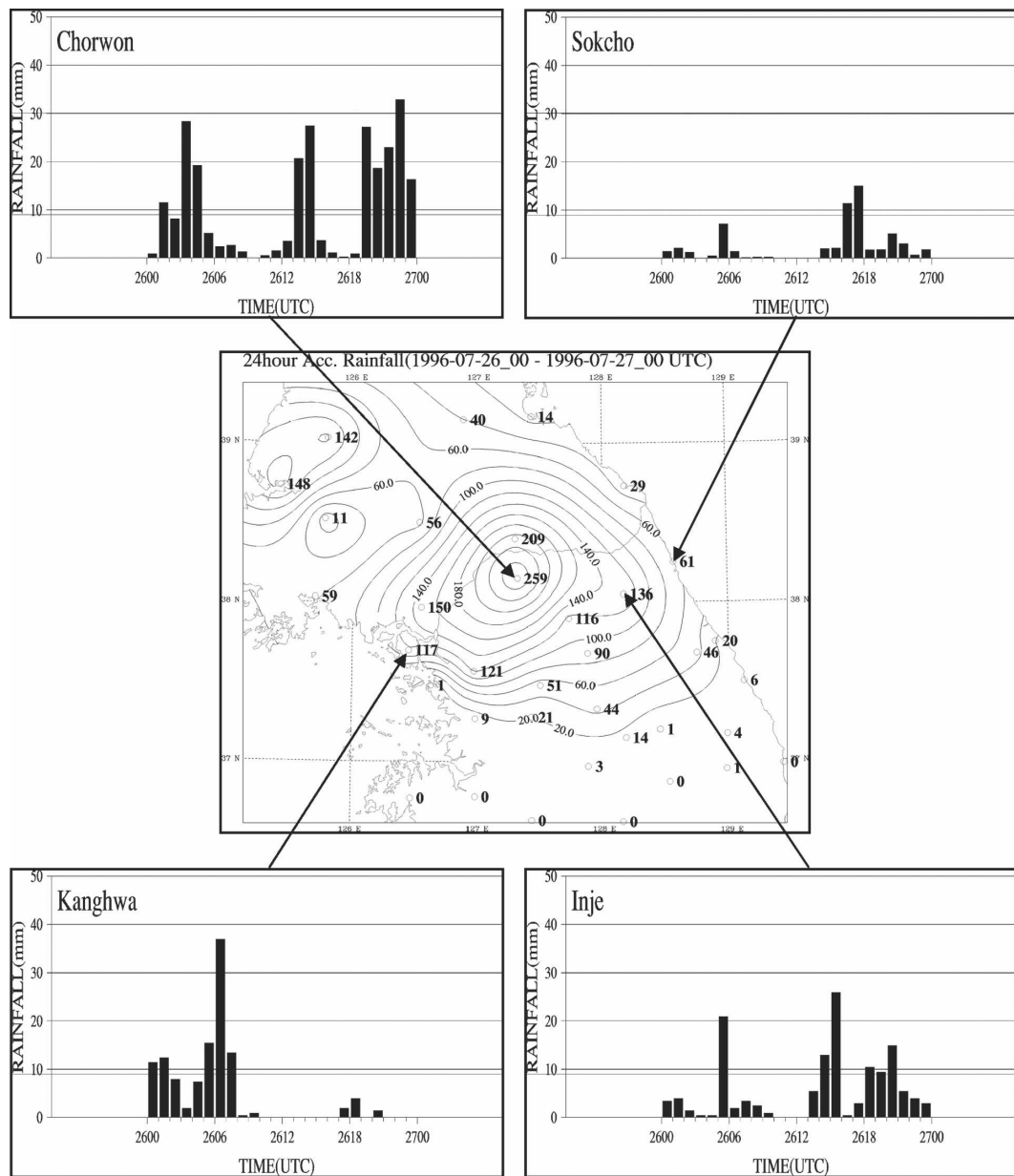


FIG. 2. The 24-h accumulated rainfall amounts over the central Korean Peninsula from 0000 UTC 26 Jul to 0000 UTC 27 Jul 1996 and temporal variation of rainfall at Chorwon, Kanghwa, Inje, and Sokcho with 1-h intervals.

are mountain ranges with modest elevations that approximately parallel the coastline. In the climatological study of heavy rainfall over Korea, Byun (1995) showed that heavy rainfall events frequently occur in the region around Chorwon. The cross section of the topography in the region (line A-B in Fig. 1) shows that the elevation from the Yellow Sea to Chorwon increases gradually with a slope of 1:500 [200 m (100 km)⁻¹], then it increases sharply to a slope of 1:100 [1000 m(100 km)⁻¹] from Chorwon to the crest of the TBM Range. The land-sea contrast and the gradual slope of the to-

pography might offer conditions favorable to the initiation and evolution of convective storms. In addition, the steep topography plays a role in preventing convective storm systems from moving eastward, making them quasi-stationary and resulting in heavy rainfall.

c. Precipitation distribution

Figure 2 shows the distribution of total rainfall amounts across the mid-Korean Peninsula together with the time series of the rain at the Kanghwa, Chorwon, Hongchon, Inje, and Sokcho stations from

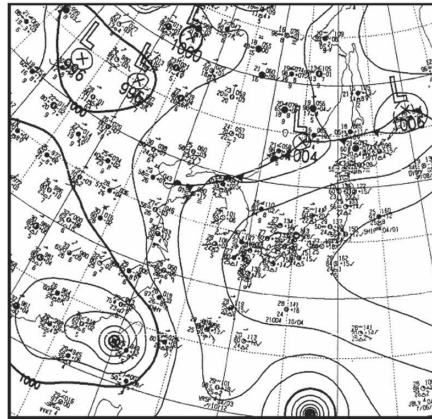
0000 UTC 26 July to 0000 UTC 27 July. The maximum amounts of total rainfall were 259 mm at Chorwon and 117 mm at Kanghwado. The precipitation amounts during the targeted period of 0900 UTC 26 July ~ 0300 UTC 27 (18 h) of this study were 243.5 mm at Chorwon, 230.8 mm at Daesung Mountain, and 103.5 mm at Inje. The maximum intensity of rainfall was 33 mm h^{-1} (2300 UTC 26 July) at Chorwon and 65 mm h^{-1} (2100 UTC 26 July) at the Daesung station (ROKAF) near Chorwon. Other stations located west and south of the Chorwon station had less than 20 mm during this period. The total precipitation amount at Paengnyongdo, Yeonpyeungdo, and Kanghwado Island was less than 5 mm for the targeted period. At the Sokcho station, located in the eastern coastal area, the 24-h rainfall amount was 61 mm. The rainfall distribution shows that the heavy rainfall was concentrated in a relatively narrow area near the DMZ and the western regions of the TBM Range. The area that experienced more than 100 mm day $^{-1}$ rainfall was approximately 40 000 km 2 in size. Hence, the heavy rainfall was caused by strong convection storms with meso- β scale or less, which initiated in the western coastal area of the mid-Korean Peninsula, not over the Yellow Sea. It also should be noted from the precipitation time series at the observation stations that there was a transition period from 0600 UTC to 1200 UTC 26 July between strong rainfall events. As will be shown in later sections, the antecedent rainfall from 0000 to 0600 UTC produced nearly saturated soil conditions and a moisture and temperature gradient field over the mid-Korean Peninsula. The low-level boundaries of temperature and moisture are important factors in the initiation of deep and moist convection. The high relative humidity values imply less entrainment of drier air into an MCS and increase the precipitation efficiency (Junker et al. 1999).

4. The environments of the MCSs

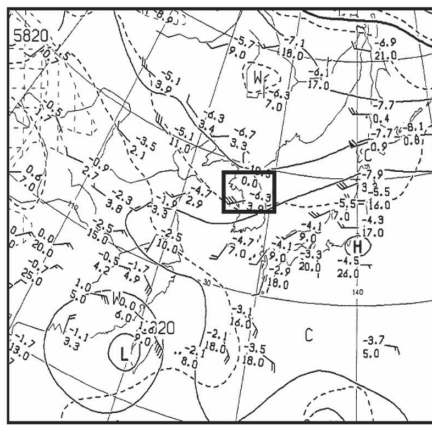
a. Synoptic conditions

Figure 3 shows the surface, and 500- and 300-hPa weather charts at 1200 UTC 26 July 1996, at approximately the time when the first MCSs responsible for the flash flooding started to organize over the central Korean Peninsula. The lower- and upper-level synoptic patterns exhibited almost the same features during the targeted period. The Korean Peninsula was on the edge of a high pressure system that extended eastward and westward over the Pacific Ocean roughly between 30° and 40°N (Fig. 3a). A quasi-stationary frontal system over northern Korea extended from a weak, low center located in the northern East Sea. Typhoon Gloria was also approaching the southeast coastal area of

(a) Surface Weather Chart at 1200UTC 26 July 1996



(b) 500hPa Weather Chart at 1200UTC 26 July 1996



(c) 300hPa Weather Chart at 1200UTC 26 July 1996

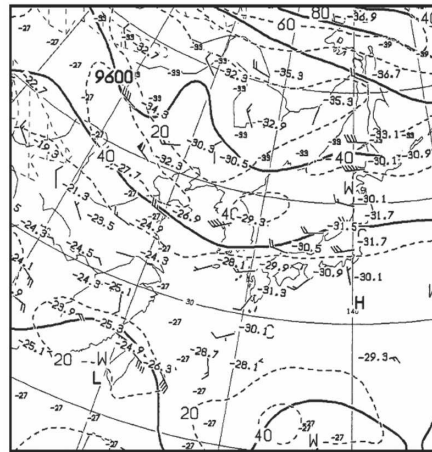


FIG. 3. (a) Surface, (b) 500-hPa, and (c) 300-hPa weather charts at 1200 UTC 26 Jul 1996. The central Korean Peninsula is shown in (b).

China, and Typhoon Herb was following the same track as Gloria. The central region of China was dominated by low pressure systems. Lee and Kim (1995) pointed out in a study of 10 heavy rainfall cases over the Korean

Peninsula that favorable synoptic backgrounds for heavy rainfall are warm advection from near the subtropical Pacific high and cold advection from northern China or Manchuria, so that strong baroclinicity builds over the Korean Peninsula and the surrounding vicinity. Thus, in this case, warm and moist air accumulated over the Korean Peninsula due to cold and dry air, establishing strong convective instabilities. Along with these conditions, more moisture was supplied from Typhoon Gloria over Taiwan, which strengthened the rainfall intensity. In the 500-hPa chart (Fig. 3b), the geopotential line height of 5880 gpm, which is regarded as the boundary of the North Pacific subtropical high in the operational analysis, intersected the central Korean Peninsula, and the 5820-gpm contour, with a weak trough, intersected the northern Korean Peninsula. The gradient of the 500-hPa geopotential height in China was very weak. At the 300-hPa level (Fig. 3c), a weak upper-level short wave accompanying a cold core in the west of the short wave developed over northeastern Manchuria. The weak upper-level jet with a 40-kt isotach line approached the Korean Peninsula from northern China. Similar to the study of Lin et al. (2001) for U.S. and Alpine cases, an upper-level short wave was also found in this case, although such upper-level short waves are typically absent in most eastern Asian cases. The 1000-hPa divergence and 850-hPa moisture advection field at 1200 UTC 26 July 1996 showed that the low-level divergent area dominated from central China to the Korean Peninsula, and the southwestern part of the Korean Peninsula was dominated by dry advection, while the northeast was dominated by moisture advection (Fig. 4). This means that the MCSs in this case were not dependent on the consequences of a synoptic-scale baroclinic system such as a front, but were the result of convection (Fritsch and Forbes 2001).

Figure 5 shows the satellite and radar reflectivity images from 1130 UTC 26 July to 0230 UTC 27 July at 3-h intervals. Clouds completely covered the Korean Peninsula throughout the entire case study period. The first MCS (A) appeared in the DMZ area at 1130 UTC and moved eastward. It was sustained for about 6 h and decayed over the TBM Range and the eastern coastal area at 1730 UTC. Rainfall intensity greater than 20 mm h^{-1} was maintained for 2 h at the Chorwon station from 1300 to 1500 UTC. At 2030 UTC, a new stronger MCS (B) occurred upstream of the first MCS. This new convection stagnated for the next 8 h and was responsible for the flash flooding over the middle portion of the Korean Peninsula. Heavy rain started at this time with rates of 30 mm h^{-1} at Chorwon and 65 mm h^{-1} at Daesung Mountain. Strong reflectivity ($>50 \text{ dBZ}$) was observed over the heavy rainfall region during this pe-

riod, and temperatures of less than -52°C spread from the western TBM Range to the East Sea. However, convective cells observed by radar remained in a limited area upstream of the MCS during the entire period, implying that the MCSs were well developed and included anvil cloud tops.

b. Storm environments

To investigate the storm environment in more detail, we analyzed the Osan sounding data. Osan is located 150 km southwest of the Chorwon station. Figure 6 shows the skew *T*-log_p and hodographs chart at 0600 UTC, 3 h before the first MCS occurred, and at 1800 UTC, just before the second MCS occurred on 26 July 1996. The severe weather parameters indicated that the environmental atmosphere was very unstable and that the lifting condensation levels (LCLs) of 679 and 763 m, and the levels of free convection (LFCs) of 685 and 361 m at 0600 and 18000 UTC, respectively, were relatively low (Table 1). There was slightly moist air located at the low and midlevels. Two moist layers were strengthened between 530 and 420 hPa and below 850 hPa. A dry and stable layer was confined between the two moist layers at 1800 UTC. The profile at this time was similar to the typical vertical temperature profile with high CAPE, associated with strong convection activity in the United States, and referred to as a "loaded gun" (Bluestein 1993). The loaded gun type of profile usually has a strong inversion or lid, and deep convection occurs where this inversion or lid is removed by some process. However, no such inversion was present in this case, and the atmosphere and only a small lifting force was needed to release its potential instability. The CAPE value was 2521 J kg^{-1} at 0600 UTC, decreased to 314 J kg^{-1} at 1200 UTC, but sharply increased to 1779 J kg^{-1} by 1800 UTC 26 July. Lin et al. (2001) mentioned that a high CAPE value is a characteristic of heavy rainfall over northeast Asia. Also, compared with operational thresholds (NWS 2004) and case studies (e.g., Stensrud et al. 1997) in the United States, the CAPE values in this study indicated high (2521 J kg^{-1}) or moderate (1779 J kg^{-1}) instability. The hodograph and wind data at 1800 UTC in Fig. 6 showed that the wind speeds below the 500-hPa level were significantly higher than those at 0600 UTC, and wind directions changed clockwise from southwesterly to westerly with height. Most hodographs actually curve in a generally clockwise manner, owing to boundary layer friction and low-level warm advection in storm cases (Bluestein 1993). The vertical wind shear is also a good indicator for predicting a storm type, as proposed by Weisman and Klemp (1986) in a study of storm evolution. When the hodograph has a clockwise direction, the storm evo-

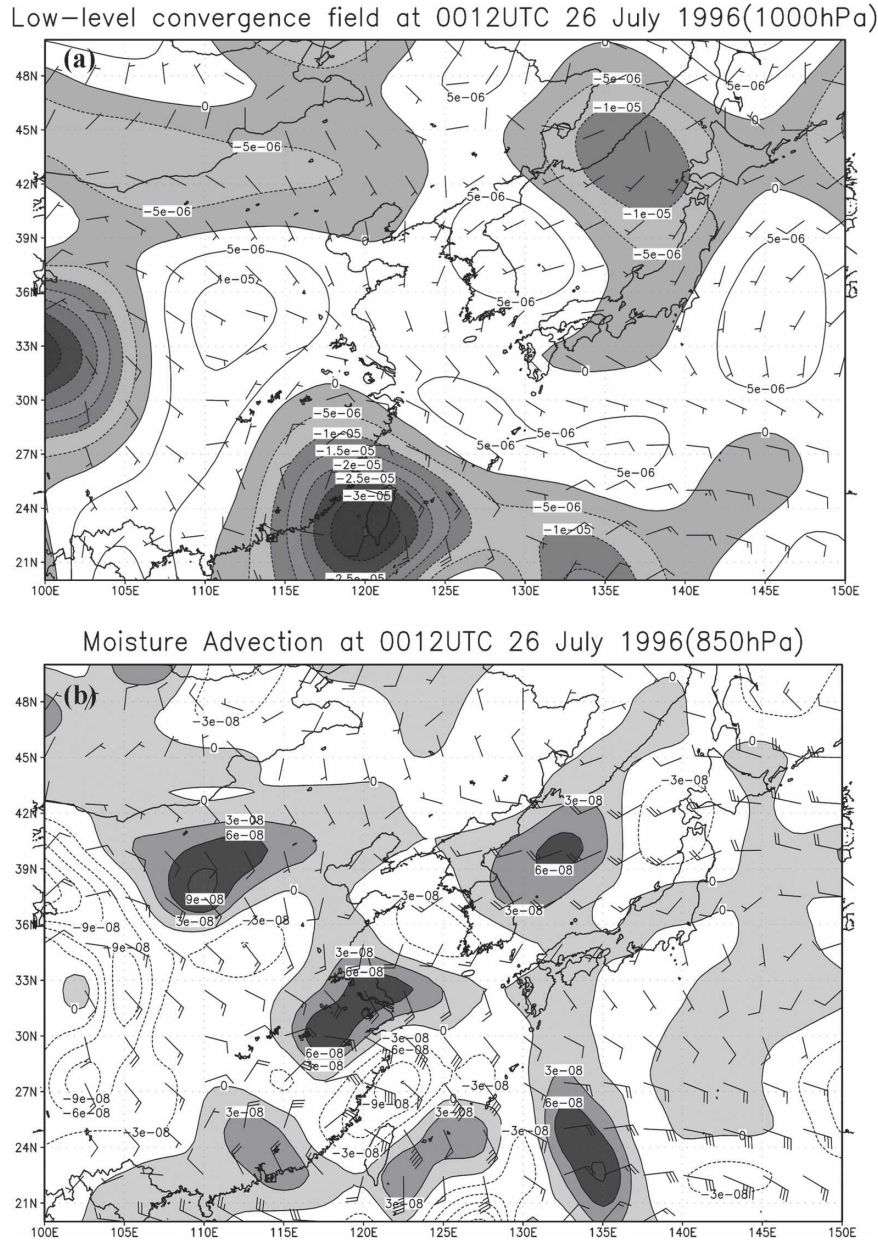


FIG. 4. NCEP-NCAR reanalysis charts for (a) 1000-hPa divergence (negative area is shaded) and (b) moisture advection at 850 hPa (positive areas are shaded) at 1200 UTC 26 Jul.

lution is directly related to the magnitude of the low-level wind shear. According to Weisman and Klemp, right-moving storms with strong wind shear develop into multicell storms by successive updraft, while storms with weak wind shear usually move leftward and decay. In this case, the bulk Richardson number (BRN) shear, the difference between mean 0–500-m wind and mean 0–6-km wind, ranged from moderate (5.8 m s^{-1}) at 0600 UTC to strong (7.8 m s^{-1}) at 1800 UTC 26 July 1996. Thus, the storms had the potential to develop as

supercell- or multicell-type storms from 0600 to 1800 UTC 26 July. Storm behavior is a function of both vertical wind shear and updraft strength, and a maximum strength of updraft is a function of CAPE. An empirical quantity, the BRN, is therefore used to predict storm type (Bluestein 1993). The BRN values in this case were 75 and 30 at 0600 and 1800 UTC 26 July 1996, respectively. Multicellular growth occurs most readily for $\text{BRN} > 30$, and supercell growth is confined to a magnitude of BRN between 10 and 40 (Weisman and Klemp

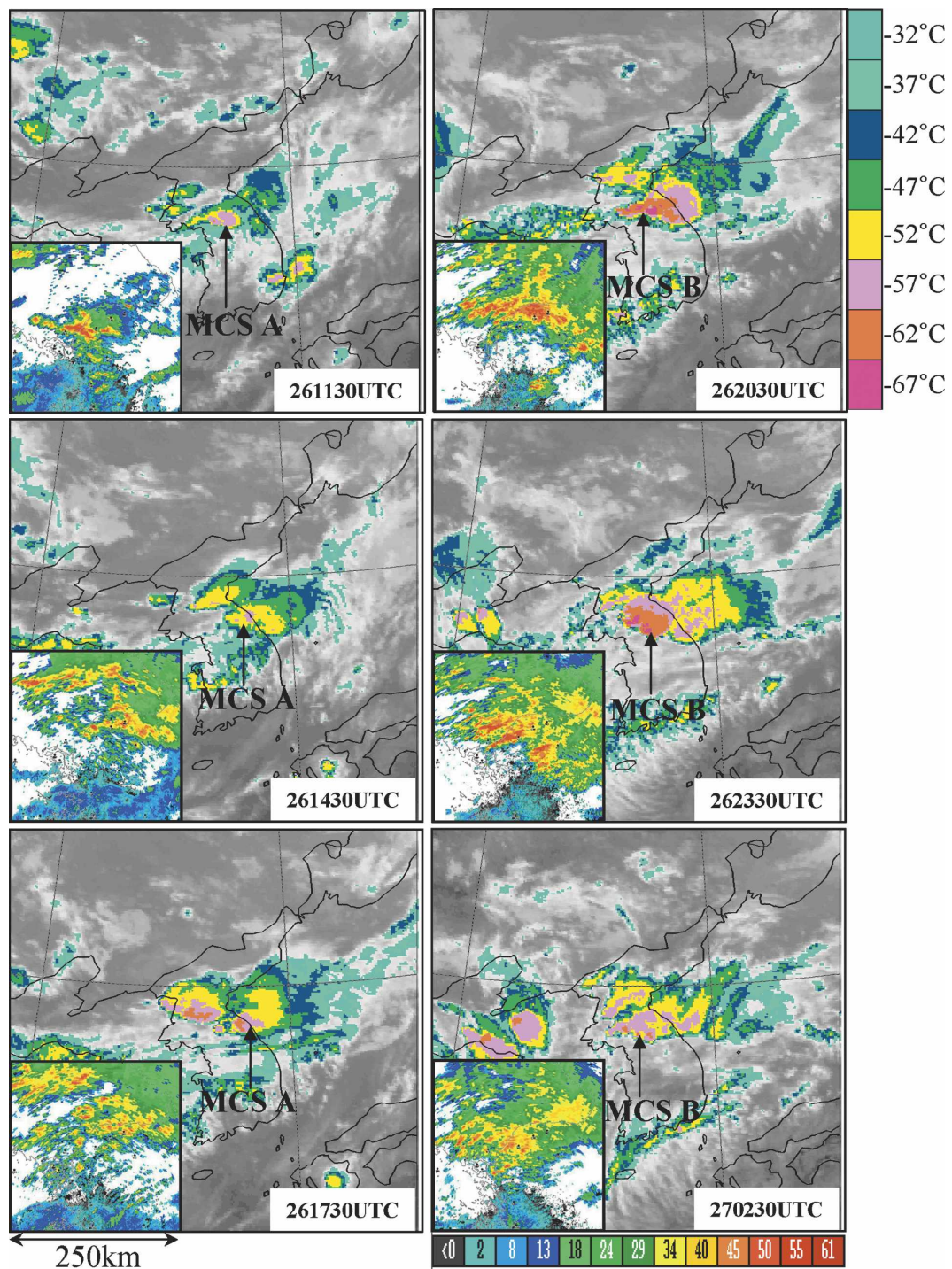


FIG. 5. GMS-5 satellite and corresponding radar reflectivity images (small squares) from 1130 UTC 26 Jul to 0230 UTC 27 Jul 1996 with 3-h intervals. Cloud-top temperatures from -32° to -67°C with 5°C intervals are shown on the right and radar reflectivity (dBZ) from 0 to 60 dBZ at 5-dBZ intervals located at the bottom.

1986). In this case, the BRN value of 30 at 1800 UTC (MCS B) was favorable for producing a long-lived multicell convective storm. The radar observations in this study also showed the typical storm types correspond-

ing to those criteria. However, the BRN value of 75 at 1200 UTC (MCS A) was not consistent with criteria in the United States, due to the relatively low BRN shear.

The time-height cross section of winds, equivalent

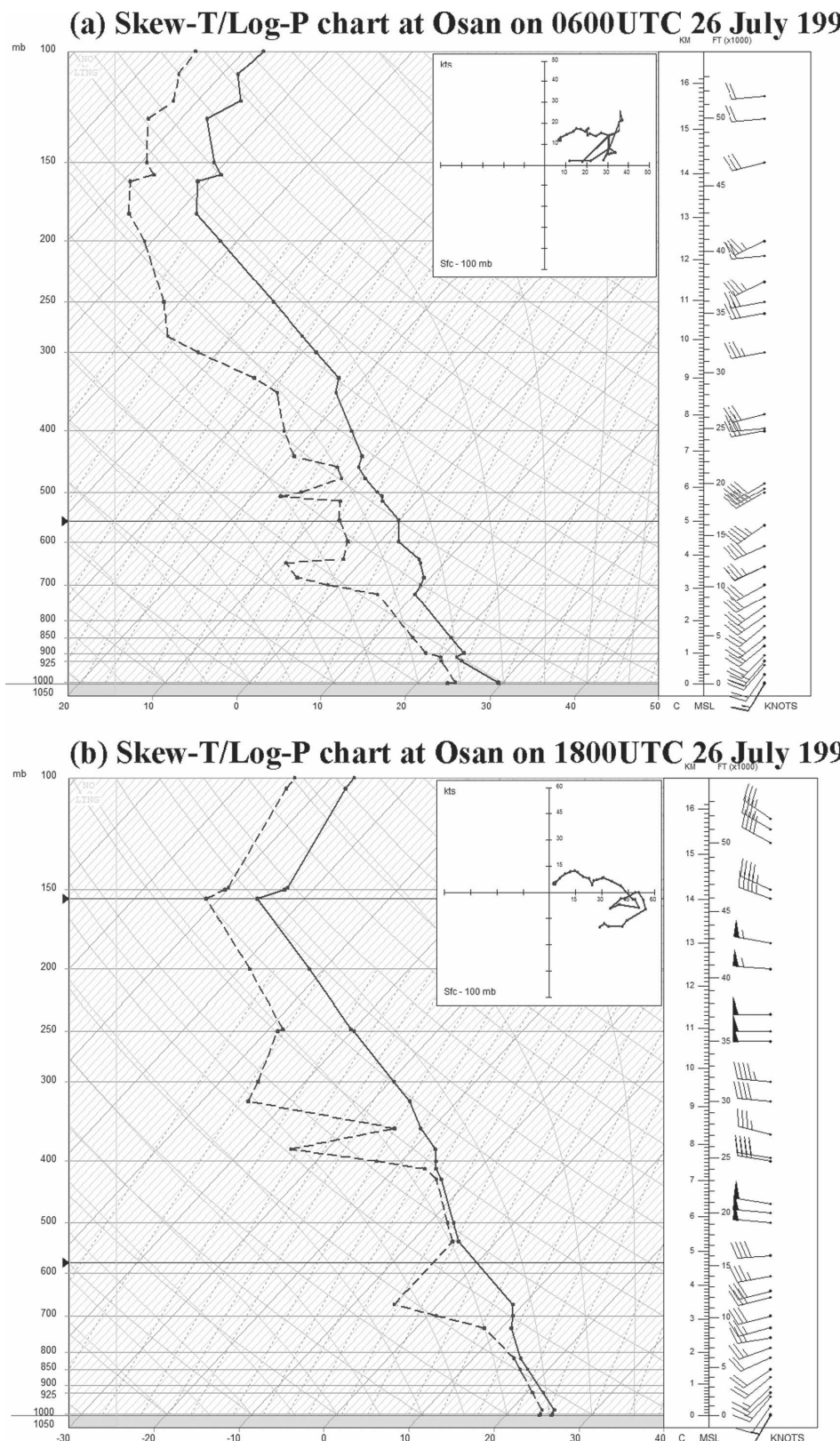


FIG. 6. The skew T -log P chart and hodography from Osan rawinsonde data at (a) 0600 and (b) 1800 UTC 26 Jul 1996.

TABLE 1. Severe weather parameters at Osan from 0000 UTC 26 Jul to 0000 UTC 27 Jul 1996. The boldface numbers indicate instability parameters at the time of new convective storm initiation.

Parameters	0000 UTC 26 Jul 1996	0600 UTC 26 Jul 1996	1200 UTC 26 Jul 1996	1800 UTC 26 Jul 1996	0000 UTC 27 Jul 1996
CAPE (J kg^{-1})	794	2521	314	1779	921
CIN (J kg^{-1})	-21	-1	-15	-7	-30
BRN shear (m s^{-1})	6.2	5.8	4.4	7.8	5.3
BRN	21	75	16	30	32
LFC height (m)	1148	686	2441	763	1294
LCL height (m)	570	679	1538	361	430
LI	-3.9	-6.3	-2.4	-6.0	-4.0
SWEAT*	284.5	317.7	333.8	393.7	320.2
Precipitable water (cm)	4.85	5.19	5.35	5.69	5.56

* Severe weather threat index

potential temperature θ_e , and relative humidity at the Osan station from 0000 UTC 26 July to 0000 UTC 27 July 1996 at 6-h intervals are depicted in Fig. 7. Relatively dry and cold air intersected between the 700- and 600-hPa levels from 0000 to 1800 UTC 26 July. While the wet and warm air was layered at low and middle levels at 0600 and 1800 UTC, the distribution of equivalent potential temperature indicated that the air was potentially unstable ($\partial\theta_e/\partial z < 0$) below 600 hPa. The high relative humidity at 0600 UTC was caused by the antecedent MCS, which passed from 0000 to 0600 UTC, and a sudden increase of relative humidity below 750 hPa at 1800 UTC seemed to be related to the transport

of warm and humid air by increased LLJ, due to increased circulation of the landfall tropical storm over southern China. The increased moisture and winds in the middle level seemed to be supported by the first MCS (MCS A at Fig. 5). The nearly saturated low and middle levels provided conditions very favorable to the development of deep convective storms (Shinoda and Uyeda 2002). Other severe weather parameters, such as lifting indices (LIs) of 6.3 at 0600 UTC and 6.0 at 1800 UTC 26 July, respectively, were sufficient to initiate convective activity compared with case studies in the United States (Weisman and Klemp 1986). With a strong LLJ of 25 to ~ 30 kt, the low-level flows in the

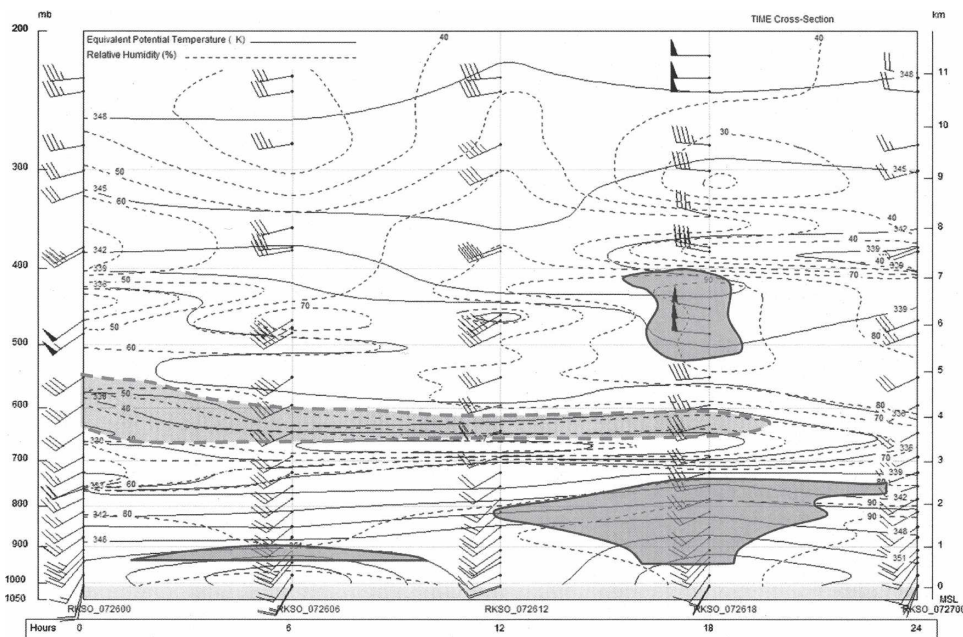


FIG. 7. Time-height cross section of wind (barb), equivalent potential temperature (K), and relative humidity (%) at Osan from 0000 UTC 26 Jul to 0000 UTC 27 Jul 1996 with 6-h intervals. The areas of humidity greater than 90% are shaded and the area less than 50% is outlined by a thick dashed line.

upstream side of the heavy rainfall region would have sufficient kinetic energy to rise above the LFC and induce conditional instability.

5. Mesoscale features in Doppler radar data

a. Storm initiation

Figure 8 shows surface analyses at 0600 and 0900 UTC 26 July. The antecedent MCS was generated at 0000 UTC and dissipated at 0600 UTC (Fig. 8a), and a new MCS initiated just after 0900 UTC (Fig. 8b). A mesoscale high pressure dominated over the central Korean Peninsula, while mesoscale low pressure was located over the southern and northern Korean Peninsula. There was a cold core collocated with the center of meso-high pressure and warm sectors with meso-low pressure systems. The central and northern Korean Peninsula region was almost saturated, while the cloud-free area in the southern peninsula was very hot and dry. These strong moisture and thermal gradients could have resulted from the antecedent MCS, which dominated from 0000 to 0600 UTC 26 July. Mesoscale boundaries such as the land–water contrast, rain-no rain areas, saturated–unsaturated soils, and steep horizontal pressure and thermal gradients can provide favorable conditions for the initiation of storms (Funk 2004). The cold air over the central peninsula resembled a cold pool created by strong outflows with precipitation from the antecedent MCS. The cold pool can persist for many hours after the decay of an MCS and often plays a role in triggering a storm in the initiation phase of successive convective storms (Doswell 2001). Figure 9 shows the time variations of surface winds at weather stations from the Yellow Sea to the east coast. The first MCS initiated around 0900 UTC in the western coastal region and coincided with the change of wind direction from west to northwest. The wind direction sustained low-level convergence over the western coastal area during this period. The second MCS initiated around 1700 UTC in the western inland area and was sustained for more than 10 h over the central Korean Peninsula. The change of wind direction from southerly to southeasterly at the Deasung Mountain station should be noted, because the easterly flow (inbound) was found in the WSR-88D data and the system movement was almost stagnant after this time. Also, the surface flow had a cyclonic circulation pattern over the inland area.

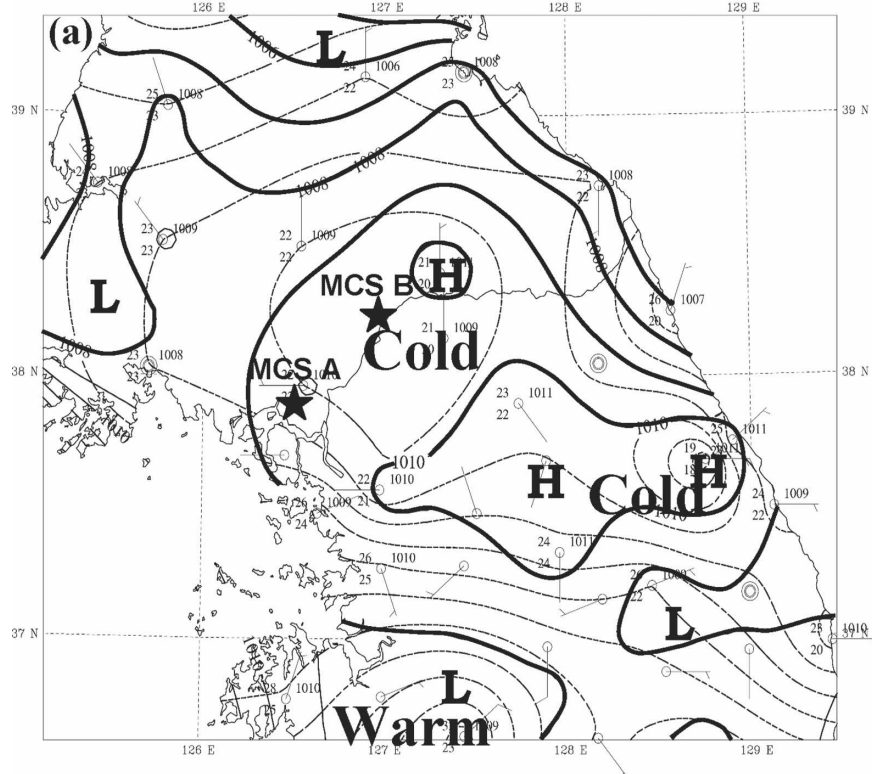
The points of the initiation of convective cells, determined by the Storm Cell Identification and Tracking algorithm in the WATADS system (Johnson et al. 1998), revealed that most new convective cells concen-

trated over the western coastal area and the western region of the TBM Range over the central Korean Peninsula (not shown). There were few identifiable convective cells over the Yellow and East Seas during the investigation period, indicating that they were generated in coastal and inland areas over the central Korean Peninsula, and the propagation of storms across the TBM Range was entirely obstructed by the highly elevated terrain. In various simulations for this heavy rainfall case, using the fifth-generation Pennsylvania State University–National Center for Atmospheric Research Mesoscale Model, the initiation of convective cells and precipitation bands was not well simulated without asynoptic data assimilation (Wee 1999; Lee and Lee 2003). Previous modeling studies using various convective parameterization schemes and four-dimensional variational data assimilation (4DVAR) show that precipitation areas organize over the Yellow Sea and successively move to the central Korean Peninsula, resulting in heavy rainfall (Wee 1999; Lee and Lee 2003). However, the model did not simulate the initiation of convective cells as shown in the Doppler radar data. In this case, the number of individual convective cells per volume-scan step resulting from the WSR-88D detection range varied from 22 to 65 during the targeted period, and the mean lifetime of individual convective cells was about 17.8 min, which is very short compared with the lifetime of MCSs.

b. Storm evolution

As mentioned when discussing the precipitation pattern, two different MCSs related to heavy rainfall occurred over the central Korean Peninsula. The first MCS initiated at 1000 UTC 26 July after a 3-h transition phase. Figure 10 shows the composite reflectivity (CR), base radial velocity (BV), and storm-relative velocity (SR) with the lowest elevation angle (0.4°) from 1000 to 1200 UTC 26 July at 30-min intervals. At 1000 UTC, nonconvective cells ($\leq 34 \text{ dBZ}$) covered the central Korean Peninsula, and no obvious convergence zone was observed in the velocity fields. The first MCS ($> 40 \text{ dBZ}$) appeared at 1030 UTC in the western coastal area along the mesoscale convergence line. Then, at 1100 UTC, the MCS abruptly developed an arc-shaped convective line accompanying an intensified convergence. After 1130 UTC, a small inbound flow (toward radar, green) developed and the mesocyclone (a yellow circle in Fig. 10d) evolved upstream of the storms (Stumpf et al. 1998). A mesocyclone within strong convection activity is a typical indicator of the occurrence of supercell storms with storm tilting (Doswell 2001). Usually, a supercell storm occurs in the United States

Meso-analysis chart at 0600UTC 26 July 1996



Meso-analysis chart at 0900UTC 26 July 1996

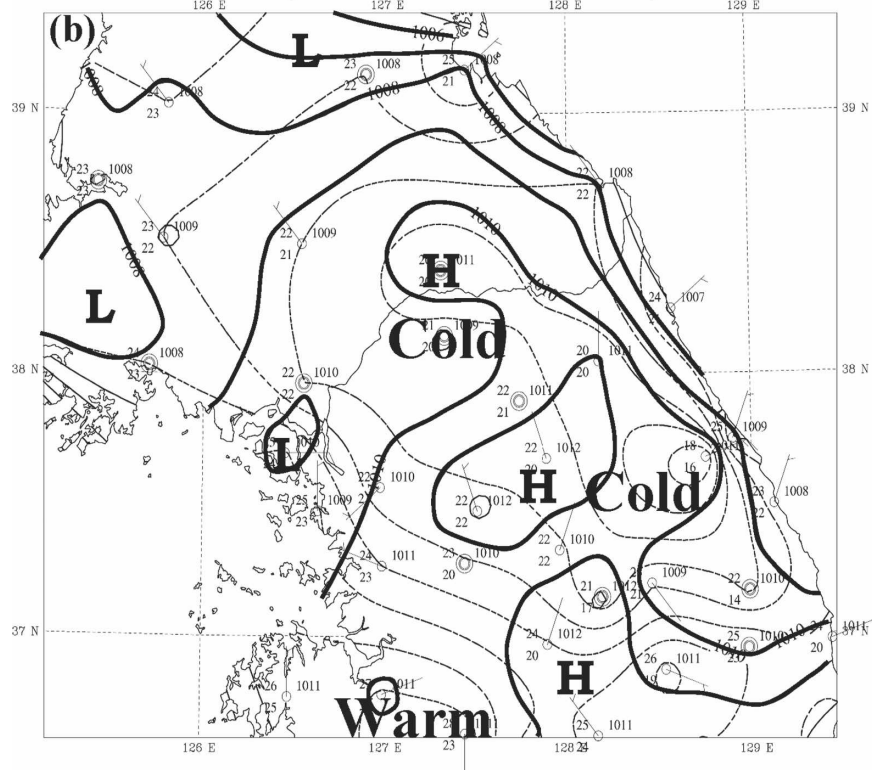


FIG. 8. The mesoanalysis chart using surface observation data at (a) 0600 and (b) 0900 UTC 26 Jul 1996. The thick solid lines denote pressure (hPa) and dotted lines temperature (°C). The filled stars (\star) denote approximate locations of the initiations of MCSs A and B.

Time variation of surface wind at weather stations

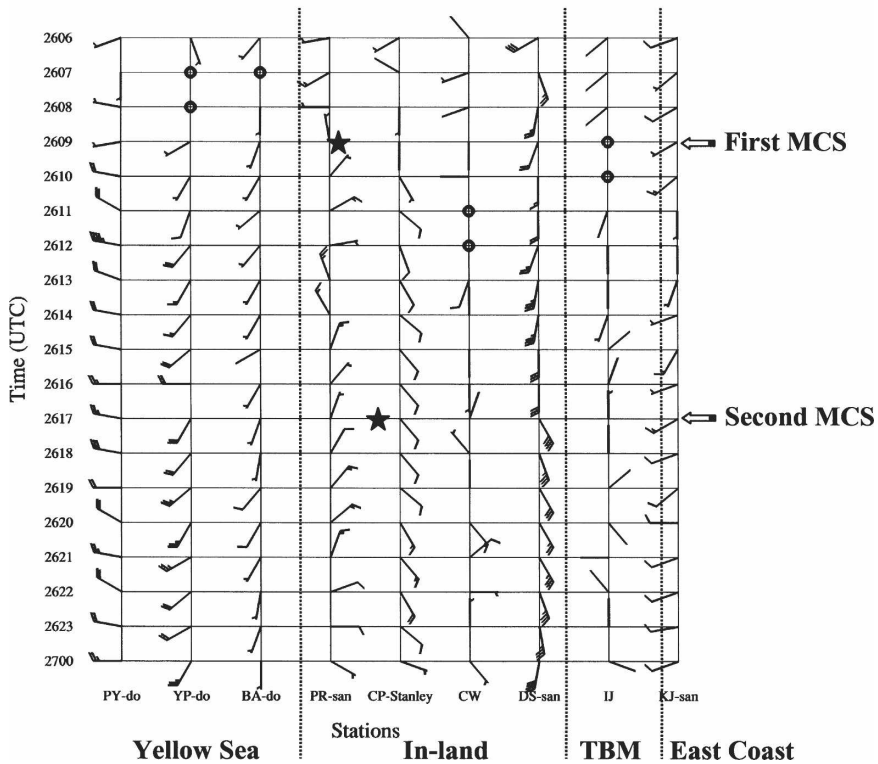


FIG. 9. Time variation of surface wind at weather stations located on an island in the Yellow Sea to the east of the coastal area: PY-do, Paekryung Island; YP-do, Yonpyung Island; BA-do, Baka Island; PR-san, Pyurip Mountain; CP-Stanley, Donduchon (U.S. Air Force); CW, Chorwon; DS-san, Deasung Mountain; IJ, Inje; and KJ-san, Kyujin Mountain. Filled stars (\star) denote approximate times and locations of the initiations of MCSs.

with significant instability with CAPE = $1000 \sim 2000 \text{ J kg}^{-1}$ and BRN less than 40. In this case, the BRN and CAPE values also satisfied these criteria.

To investigate the time evolution of the supercell storm in more detail, we constructed the cross section of reflectivity and BV perpendicular to MCS movement (north-south) following the strongest storm in the MCS at 10-min intervals from 1030 to 1100 UTC and from 1130 to 1200 UTC (Fig. 11). The convective storms were well developed horizontally and vertically with outbound flow (red) appearing below 5-km elevation and at the upper level of the storm at 1030 UTC. The weak inbound flow appeared at the midlevel of the storms, and the width shrank to 20 km at 1130 UTC. The midlevel rear-to-front jet developed and reached to the bottom of the storm. In the meantime, the convective storm grew to over 10 km at 1150 UTC. Figure 12 shows the detailed structure of a supercell-type storm at 1150 UTC following line E-F in Fig. 10. The reflectivity showed that the convective line had a meso- β scale with a 20-km-wide convective region and

a 5-km width at the strongest convection core. The convective core reached 8-km altitude, and the top of the storm exceeded the tropopause level. A weak echo region (WER) also appeared from 5 to 8 km. A WER occurs when a great number of precipitation particles reach aloft by strong updraft flow; therefore, the existence of a WER is a good indicator of storm severity (UCAR 2002). The cross section of BV showed that the storm was tilted to the north, and a cyclonic rotating vortex (mesocyclone) was connected with the updraft located below 5 km and divergent flow with an anticyclonic vortex near the top of the storm. The cross section of SR portrayed the structure of the storm-relative flow during the evolution of the storm. The front-to-rear (F-R) flow collided with the leading edge of the convective storm and moved aloft of the storm, and then part of the F-R flow returned toward the front and remained flow off at the rear edge of the storm. A rear-inflow jet (RIJ), one indicator of a mature storm, was also observed at the midlevel of the storm. One of the most important roles of the RIJ is to ensure lon-

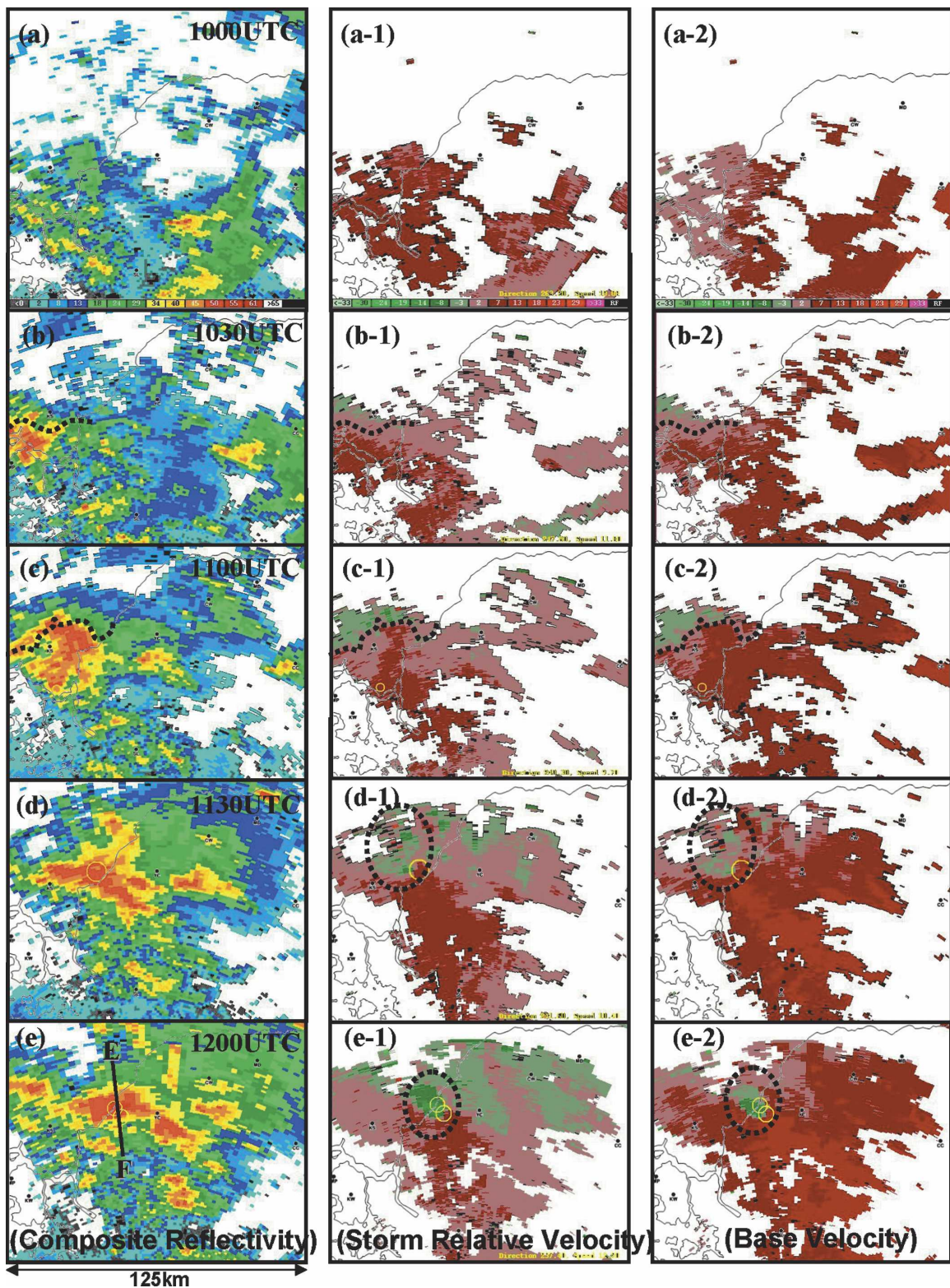


FIG. 10. The CR (left), SR (middle), and BV (right) from (a) 1000 through (e) 1200 UTC 26 Jul 1996 in 30-min intervals, respectively. The green colors denote inbound (toward radar), while the red colors refer to outbound (away from the radar), and the yellow circles in thick dashed lines in (d) and (e) denote mesocyclone activities.

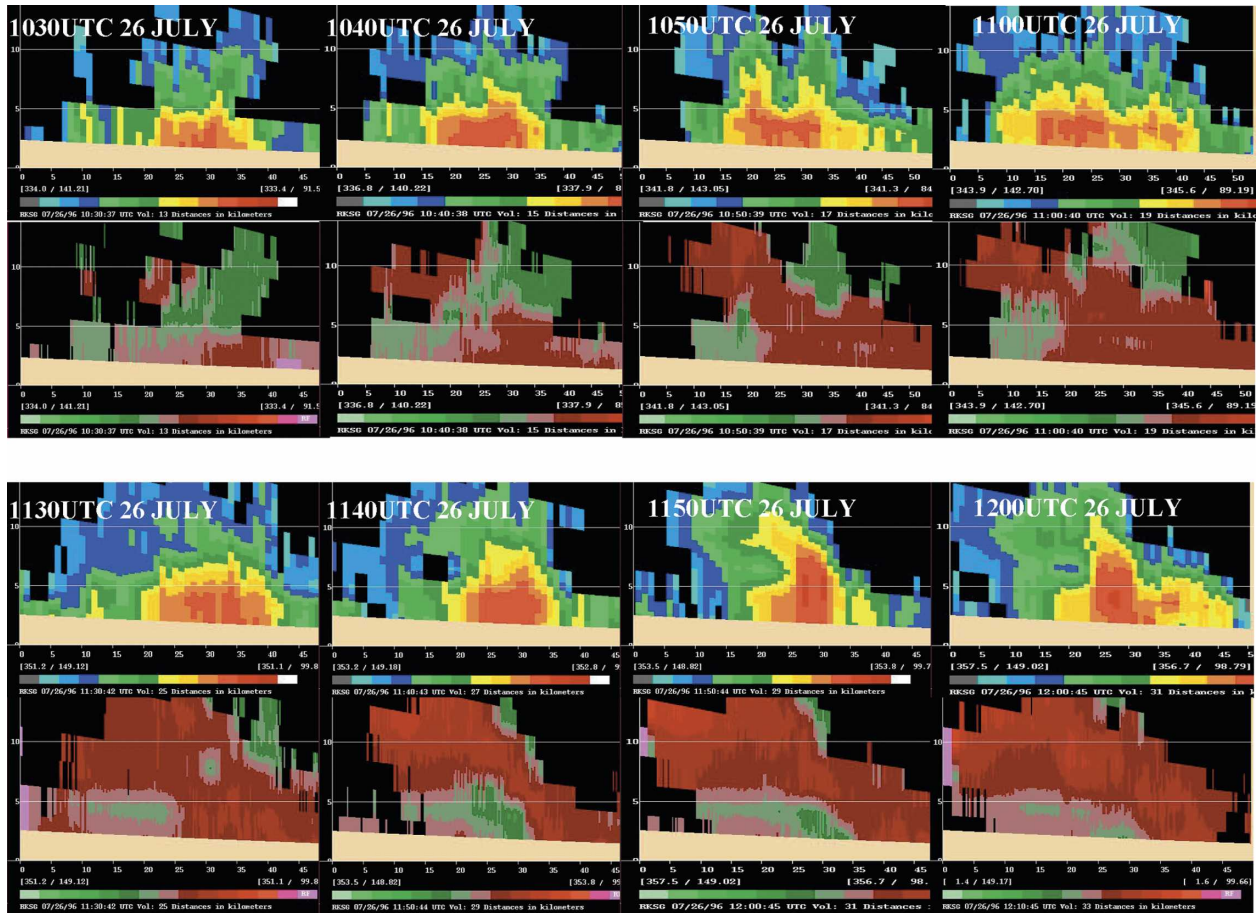


FIG. 11. The cross section of reflectivity and base velocity perpendicular to MCS movement (north–south) following the strongest storm in the MCS from 1010 to 1230 UTC at 10-min intervals.

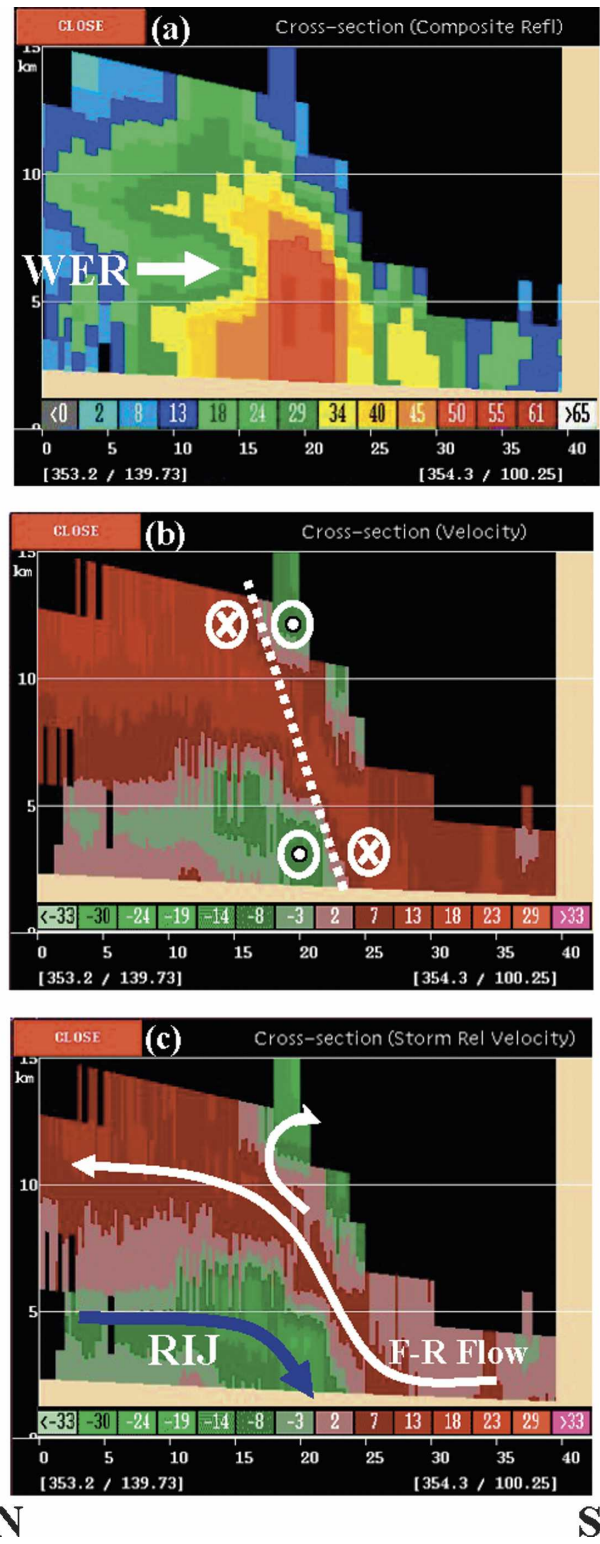
gevity of a storm system by halting its decay (Weisman 1992).

After the first MCS passed, at 1800 UTC 26 July, convective storms of moderate to heavy intensity were scattered over the central Korean Peninsula (see Fig. 15). The individual storms consolidated over time and finally formed a single squall line at 1931 UTC 26 July, resembling a “broken areal” squall line (Bluestein and Jain 1985). The broken areal formation process may be developed along the cold outflow boundaries between existing convective cells (Weisman and Klemp 1984). The environmental condition in this case corresponded well to the broken-areal-type characteristics. Compared with the first MCS, there was no low-level convergence zone or mesocyclone during the initiation and evolution period. The low-level convergence zone and mesocyclone were observed in the fully mature stage of the MCS. The second MCS was somewhat more severe during the squall line evolution phase than the first supercell-type storm was, but resulted in more heavy rain-

fall over the targeted region due to slow or quasi-stationary movement.

c. Storm movement and propagation

The pattern of storm movement and propagation can control the amount and location of heavy rainfall. The motion of a storm system consists of two vectors: the mean velocity of individual cells and the propagation velocity due to the formation of new cells on the periphery of the storm (Chappell 1986). Propagation refers to the apparent movement of a convective system due to the development of new cells on their flank, where moist, unstable inflow air is present. The main types of propagation include forward, quasi-stationary, backward, and regeneration (Funk 2004). The pattern of storm propagation in the two MCSs of this case study was investigated using a time–height cross section of reflectivity and BV with 30-min intervals. The cross section was constructed along the line (southwest–northeast) where the most significant convective activi-



N

S

FIG. 12. The cross section of (a) reflectivity, (b) base velocity, and (c) storm-relative velocity at 1150 UTC 26 Jul 1996 along the line E–F shown in Fig. 10e. In (b), the circle with a dot (\odot) denotes the wind direction out of the page, and the crossed circle (\otimes) denotes the wind direction into the page.

ties were detected from WSR-88D data. Figure 13 shows the time–height cross section of the first MCS from 1000 to 13000 UTC and the second MCS from 2200 26 July to 0100 UTC 27 July, with 30-min intervals. The new storms in the first MCS were generated downstream of the leading edge of the convective storm, and the entire system moved northeastward relatively rapidly. In contrast, the new storms in the second MCS were initiated upstream of the leading convective storms, and storm movement was very limited overall. The westerly flow dominated from the bottom to the top of the storms in the first MCS, except for a mesocyclone at low and middle levels (white dotted circle in Fig. 13), while the strong middle-level westerly flow (red) and low- and upper-level easterly flows (green) dominated in the second MCS. The vertical wind shear with a middle-level jet seemed to play an important role in the development of the quasi-stationary, multicell storms. To investigate the movement and propagation of the storms, we tracked the edges of the convective storms (Fig. 14). As mentioned above, the two MCSs showed very different patterns of storm movement and propagation. The first MCS (1000 ~ 1800 UTC 26 July) was of the forward propagation type, in which new cells occur on the downstream leading edge, followed by the merging of new cells to the MCS (Fig. 16a). The storm system (CS) moved slowly northeastward at 8 m s^{-1} , and the mean speed of individual cells was 14.9 m s^{-1} in the general direction of the main storm system. The propagation vector (PS) was relatively weak. Typically, supercell-type storms move quickly (Chappell 1986). The second MCS that initiated around 1800 UTC showed a propagation pattern that was very different from the first. The convective line (Fig. 15b) extended from the west coast to the TBM Range during the initial phase. However, the eastern edges of the convective line shrank westward as the MCS developed. The storm system (CS) moved southeastward, approximately perpendicular to the mean direction of the individual cells (CC), at a speed of 3.2 m s^{-1} . The mean speed of the individual cells was 14 m s^{-1} , which was almost the same as that of first MCS. The propagation vector (PS) of the second MCS was much stronger than that of the first. Its convective lines were variable, and the MCS had quasi-stationary or backward propagation. Under these circumstances, new storms developed successively upstream of the MCS, and provided suitable conditions for flash flooding.

Figure 15 shows the CR to be greater than 40 dBZ from 1800 UTC 26 July to 0300 UTC 27 July, with 1-h intervals. A 1-h interval was too long to track individual cells because of their short life cycles ($\approx 17.8 \text{ min}$), but was sufficient to track the movement and clustering of

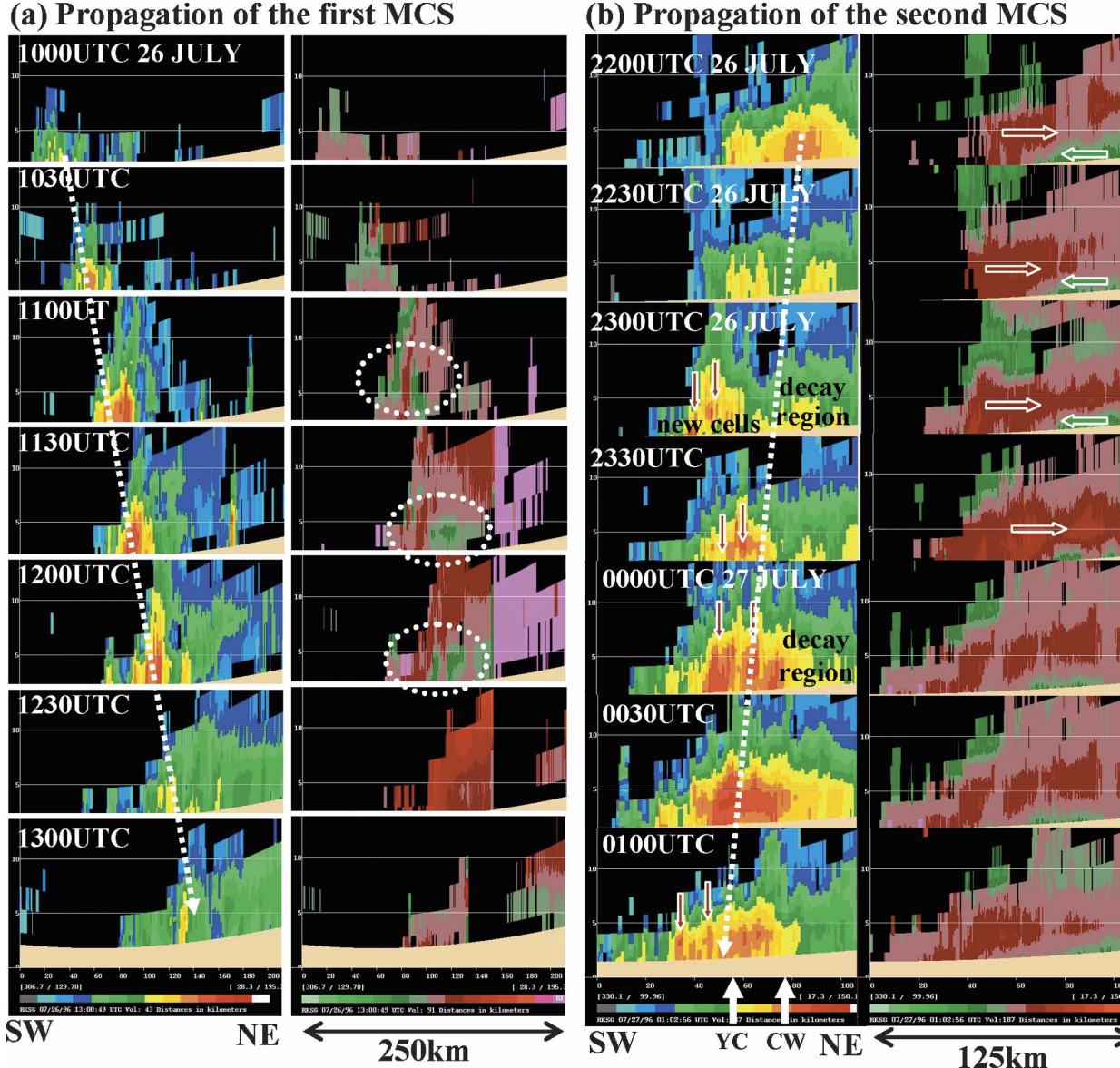


FIG. 13. The time-height cross section of reflectivity and base velocity along the line of the most significant convective activities (southwest–northeast) (a) from 1000 to 1300 UTC 26 Jul 1996 and (b) from 2200 UTC 26 Jul to 0100 UTC 27 Jul with 30-min intervals, respectively. The white dashed arrows denote the propagation directions of storms and the white circles denote regions where a mesocyclone activated. Open arrows denote the direction of flow.

the storms. We designated an area as a “storm cluster” if it included convective storms of more than 40 dBZ, and numbered each cluster. When small clusters merged into a big cluster, a capital letter was assigned. After a large cluster formed, the individual storms in the cluster were designated by a lowercase letter to track the merging process.

The scattered, small clusters (1801 UTC) merged slowly to generate a large cluster A, just north of Chorwon at 1900 UTC (Fig. 15b). The observed data at Chorwon showed strengthened precipitation intensity,

and at that time a thunderstorm occurred. The small clusters, 1 and 10, merged into a large cluster B, (2000 UTC), and eventually clusters A and B merged into a single cluster C at 2100 UTC 26 July. Cluster C had horizontal dimensions of 50 km × 200 km and included strong convective storms (a + b + c, g, and h). The eastern edge of cluster C gradually shrunk, and its further eastward movement was obstructed after 2200 UTC 26 July. However, small but violent storms (j, k, l, and n) occurred sequentially in cluster C. Cluster C separated into clusters D and E at 0100 UTC 27 July

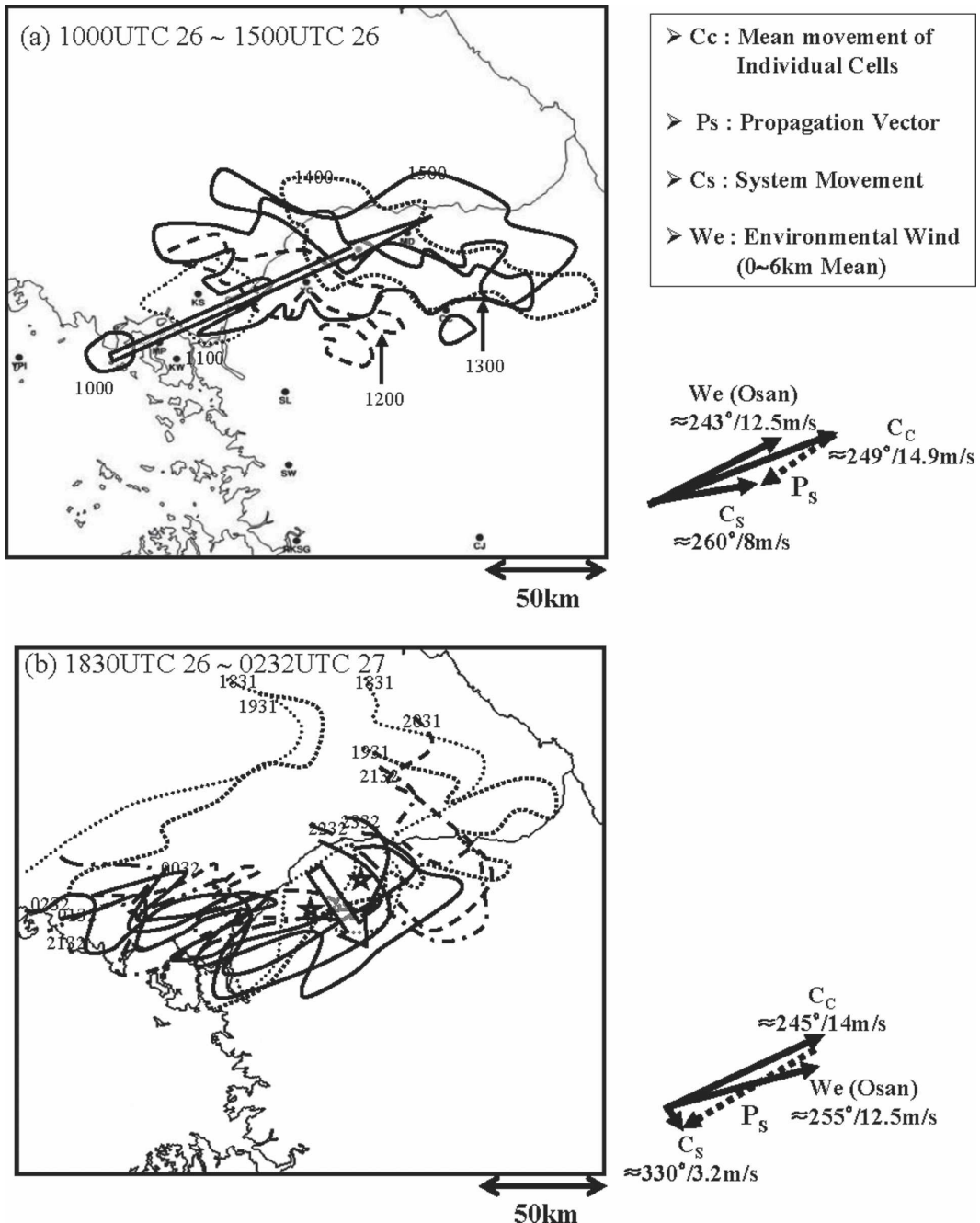


FIG. 14. The convective storm boundaries (a) from 1000 to 1500 UTC 26 Jul 1996 for the first MCS, and (b) from 1801 UTC 26 Jul to 0232 UTC 27 Jul for the second MCS. The open arrows with light shading show the temporal changes of the boundaries. The thick arrows on the right denote the mean movement of individual cells (CC), the movement of the storm system (CS), the propagation vectors (PS), and the environmental wind speed resulted from Osan rawindsonde data (WE).

and then decayed at 0300 UTC. The sequential and intensive storms in the large clusters had relatively long lifetimes (~ 2 h) and directly affected the flash floods in Yonchon and the Imjin River basin, in the early morning of 27 July 1996. The TBM Range likely played a

role in blocking the eastward movement of the convective clusters. The clusters were well resolved on the far western side of TBM Range (slope $\approx 1/500$). However, when the leading storm moved farther eastward and approached the steep area (slope $\approx 1/100$) of the TBM

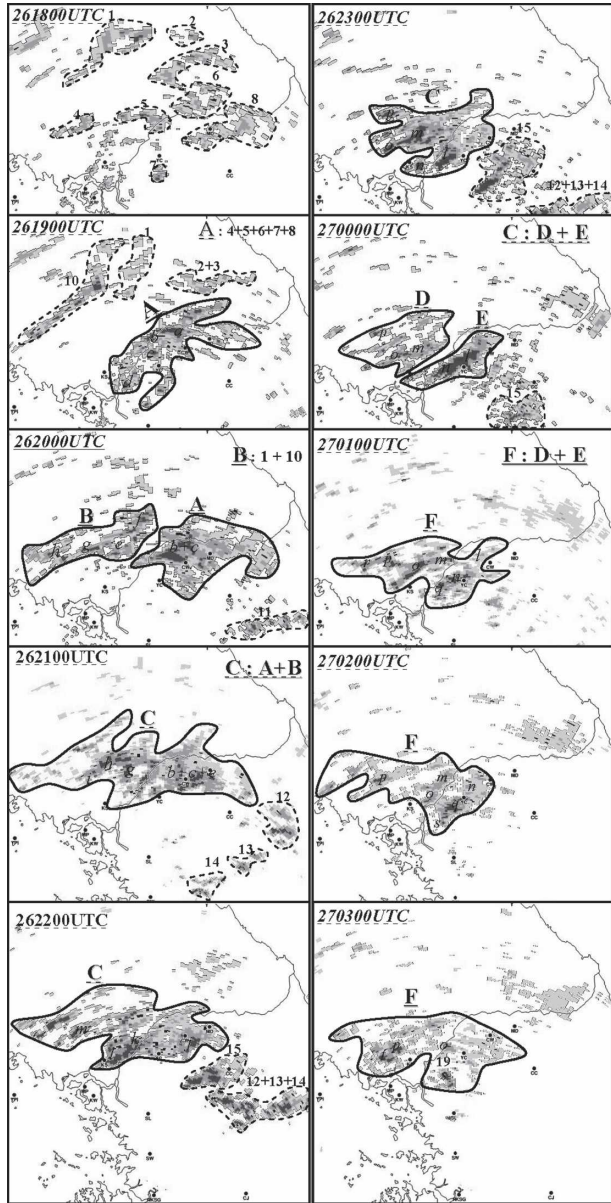


FIG. 15. Composite reflectivity of greater than 40 dBZ from 1800 UTC 26 Jul to 0300 UTC 27 Jul 1996 at 1-h intervals. The dotted lines represent small clusters and the solid lines represent large clusters. The numbers in the clusters denote small convective cells.

Range, it stagnated and new storms merged into the leading storm to build a large cluster.

d. Structure and kinematics of MCS

The temporal change of storms is useful in assessing the potential of heavy rainfall and the characteristics of kinematics in MCSs. Figure 16 shows the time-height section of reflectivity, base velocity, storm-relative ve-

locity, and vertically integrated liquid (VIL) with 10-min intervals over Yonchon from 2100 UTC 26 July to 0303 UTC 27 July. The reflectivity values greater than 40 dBZ are shaded. The dashed lines with negative values indicate easterly flow, while the solid lines and positive values indicate westerly flow. The minimum detectable height with the lowest elevation angle (0.4°) was 1.9 km at Yonchon, due to the distance from the WSR-88D site to Yonchon (118 km). The reflectivity values were greater than 20 dBZ for the whole period at the points. The convection storms had lifetimes ranging from 10 to 150 min. A major storm with a long lifetime of 150 min dominated the Yonchon area. The strongest reflectivity value was 51 dBZ over Yonchon. Those values were relatively low compared with a published case of heavy rainfall and a hailstorm that occurred in the United States (Lemon 1998), but about equal to or higher than those of a heavy rainfall event during the baibu period over Japan and the East China Sea (Watanabe and Ogura 1987; Moteki et al. 2004a). The region of strong convection (≥ 40 dBZ) accumulated below the freezing level, and the core of reflectivity was located at lower than 4.0 km over Yonchon. Usually, a lower cloud-base height decreases evaporation in the subcloud layer, and an accumulation of higher cloud liquid water under the freezing level enhances the precipitation efficiency by the collision-coalescence (warm rain) process. In this study, the VIL values that were sharply changed corresponded to the initiation and decay of storms.

The temporal variation of the reflectivity and the radial velocity field over Yonchon shows the characteristics of long-lived severe storms. Just before the convective storm developed suddenly and grew above the tropopause level (2352 UTC 26 July), strong easterly flows (negative values) were observed. Moreover, the midlevel westerly jet developed at 6 km, while the upper-level diffluent flow appeared at approximately 12 km. The strong storm-relative inflow enhanced moisture convergence at lower levels, and the moderate-to-high vertical wind shear in the storm led to slow movement and halted the decay of the storms due to decreased entrainment. This kind of reflectivity and this velocity pattern were important for the long-lived storms.

e. Precipitation derived from WSR-88D reflectivity

Figure 17 shows the spatial distribution of 3-h precipitation amounts derived from WSR-88D reflectivity data using the reflectivity–radar rain rate ($Z-R$) relationship as $250R^{1.2}$ in the WSR-88D rainfall algorithm (Fulton et al. 1998) from 0930 to 1830 UTC 26 July and from 1800 UTC 26 July to 0300 UTC 27 July. The pre-

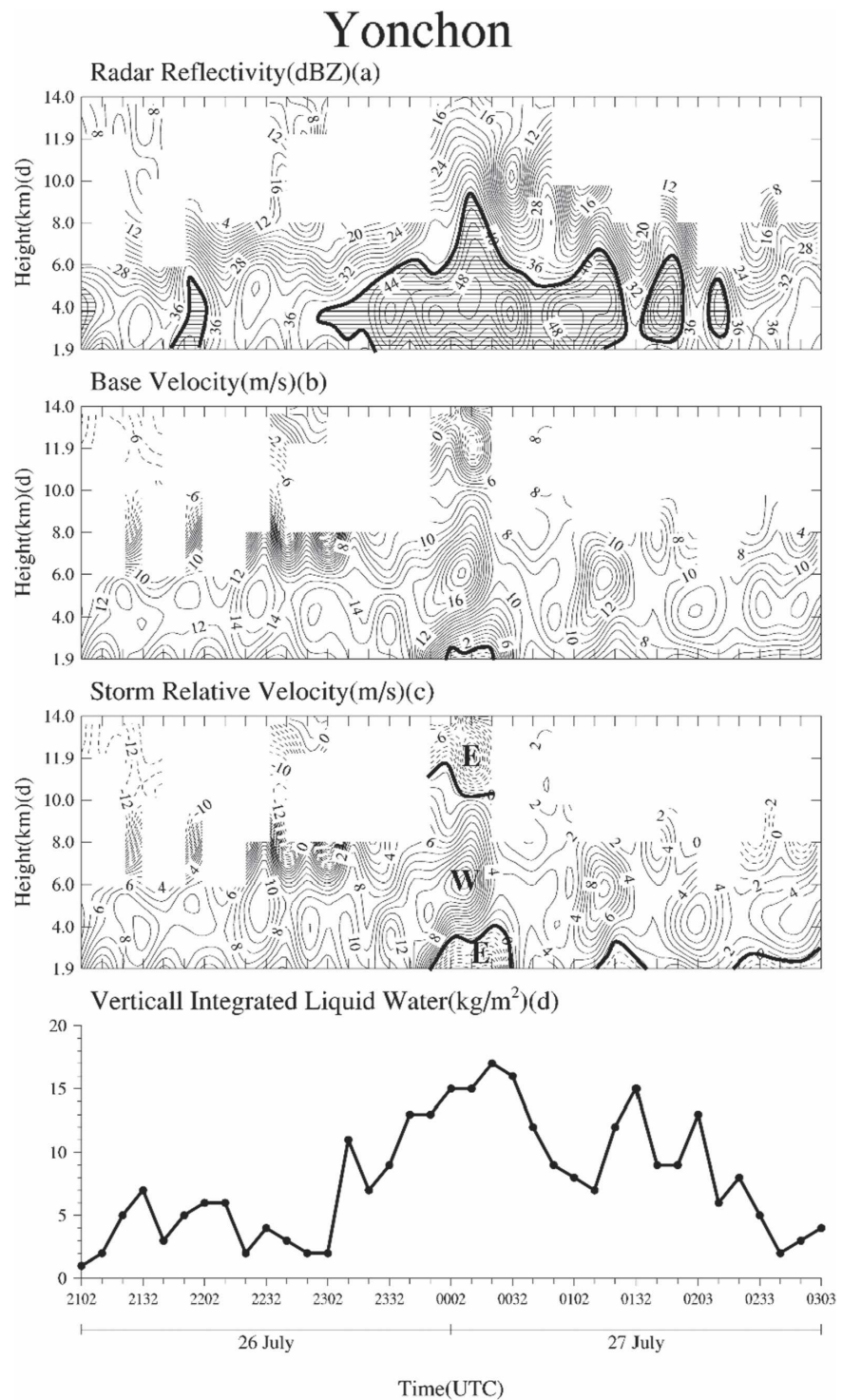


FIG. 16. Time-height section of (a) reflectivity, (b) base velocity, (c) storm-relative velocity, and (d) VIL over Yonchon from 2102 UTC 26 Jul to 0303 UTC 27 Jul 1996. The regions with reflectivity values greater than 40 dBZ are shaded and negative values in the velocity field (easterly) are depicted by dotted lines.

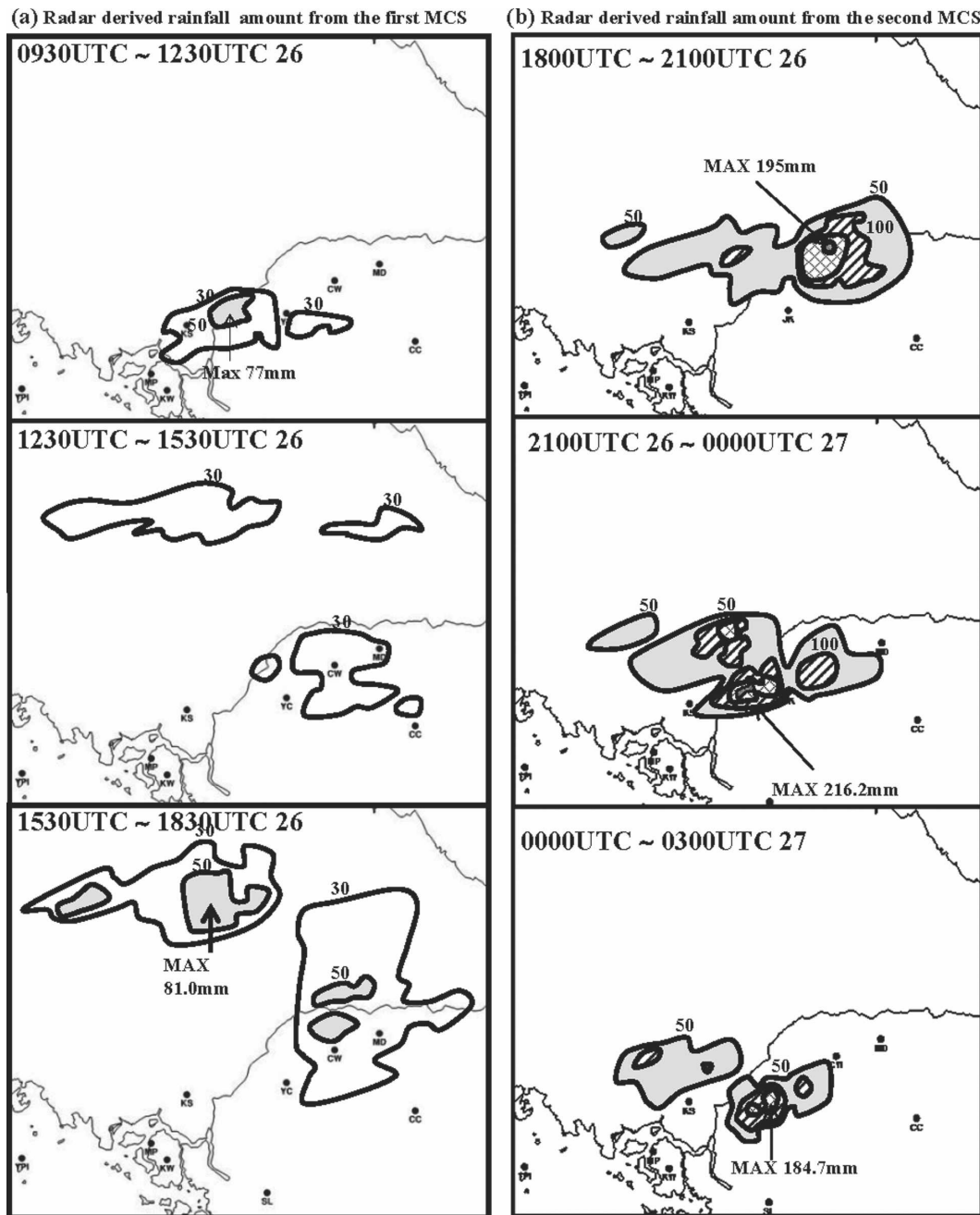


FIG. 17. The 3-h accumulated rainfall amounts derived from WSR-88D reflectivity data with a $Z-R$ relationship of $250R^{1.2}$ for (a) the first MCS from 0930 to 1830 UTC 26 Jul 1996 with 20-mm intervals and (b) the second MCS from 1800 UTC 26 Jul to 0300 UTC 27 Jul 1996 at 50-mm intervals. The areas greater than $50 \text{ mm} (3 \text{ h})^{-1}$ are shaded. (Also, refer to Table 2.)

cipitation pattern and amount of the first MCS corresponded to the characteristics of low-precipitation (LP) supercell-type storms (Moller 2001) with a maximum 3-h accumulated precipitation amount of 81 mm and relatively rapid eastward movement of precipitation centers. On the other hand, the precipitation pattern of

the second MCS showed the characteristics of quasi-stationary or backward-propagated MCSs, and the maximum 3-h accumulated precipitation was 216.2 mm. Comparing the surface-observed precipitation amounts (Fig. 2), the center of precipitation shifted westward, corresponding to the actual flash flood regions near

TABLE 2. The 3-h accumulated rainfall amounts (cm) from surface stations and WSR-88D using a $Z-R$ relationship of $250R^{1.2}$.

	0900–1200 UTC 26 Jul 1996	1200–1500 UTC 26 Jul 1996	1500–1800 UTC 26 Jul 1996	1800–2100 UTC 26 Jul 1996	2100 UTC 26 Jul–0000 UTC 27 Jul 1996	0000–0300 UTC 27 Jul 1996	Total
Chorwon (WSR-88D)	2.3 (12.2)	51.8 (67.8)	5.3 (17.5)	46.9 (140.8)	72.3 (119.1)	43.2 (51.6)	221.8 (408.9)
Deasung (WSR-88D)	4.1 (4.6)	34.9 (67.8)	36.2 (12.4)	100.6 (120.4)	24 (109.5)	22.3 (41.4)	222.1 (356.1)
Chunchon (WSR-88D)	6.7 (4.8)	13.5 (12.9)	0.7 (1.0)	0.8 (1.3)	38.8 (26.4)	22.2 (5.0)	82.7 (51.44)
Sokcho (WSR-88D)	0.5 (0.2)	2.1 (3.3)	28.8 (8.6)	8.9 (2.5)	5.8 (5.3)	11.7 (1.5)	57.8 (21.51)

Yonchon and the Imjin River basin. Table 2 shows a comparison of the 3-h accumulated rainfall amounts from surface observations with radar-derived rain amounts at Chorwon, the Daesung Mountain station, Chunchon, and Sokcho from 0900 UTC 26 July to 0300 UTC 27 July 1996. The 3-h accumulated rainfalls from the surface observations and radar for the first MCS agreed relatively well. However, the rainfall amounts for the second MCS differed significantly, especially at Chorwon and Daesung Mountain. The observed precipitation amounts at Chorwon and Daesung Mountain were about half of the radar-derived values, and there were significant differences in the 3-h rainfall amounts at Chorwon (from 1800 to 2100 UTC 26 July) and at Deasung (from 2100 UTC 26 July to 0000 UTC 27 July 1996). Seo et al. (2000) explained that the range-dependent bias during radar rainfall estimation is possibly due to poor radar data such as nonuniform vertical profile of reflectivity and that mean-field bias is caused by uncertainties in the $Z-R$ relationship. We also suppose that these differences might be a result of the size of the convective storms. Surface observations only represented point values, whereas the radar-derived data were calculated using areal mean reflectivity values and possibly captured the convective storms. Unofficial reports from the local government office show that the 24-h rainfall amount exceeded 500 mm at Yonchon and the Imjin River basin in the early morning of 27 July 1996. This matched the derived precipitation amounts—about 400 mm for 8 h over Yonchon and the Imjin River basin (Fig. 17b). The derived rainfall from WSR-88D showed that the storms were successively generated upstream of the preexisting system (backward propagation) from 1800 UTC 26 July to 0300 UTC 27 July 1996. Even though the $Z-R$ relationship should be carefully calibrated based on a climatological survey, the derived precipitation amount from radar reflectivity might be a good alternative tool for a data-sparse region.

6. Conclusions

This study analyzed the characteristics of the MCSs accompanying heavy rainfall, based on Doppler radar

data, synoptic data, and the storm environment from 26 to 27 July 1996. The quasi-stationary surface front, the abundant moisture support from a typhoon landfall in China, preexisting precipitation, and southwesterly LLJ conditions were the main synoptic-scale factors identified as causing convective instability and heavy rainfall over the central Korean Peninsula. However, directly imposed forcing like synoptic-scale, low-level convergence, which usually develops in most heavy rainfall events in Korea and generates upward motion and triggers a deep convective storm, was not found through the synoptic-scale investigation. The storm environmental conditions showed that the wet and warm air at low levels and dry and cold air at midlevels, along with previous precipitation, transport of moisture by LLJ-provided potentially unstable conditions, and the low height of the LCL and LFC, were enough to initiate deep convection by small upward motion. However, the mesoanalysis of surface pressure, temperature, and wind showed that mesoscale boundaries such as rain-no rain area, saturated-unsaturated soil, strong horizontal temperature and moisture gradients caused by the antecedent MCS, and low-level convergence on the coastal area could provide favorable conditions for the initiation of storms over the central Korean Peninsula. Hence, the deep convective storm was initiated by mesoscale forcing such as a cold pool, a mesoscale convergence line, terrain, and surface boundaries. Most new convective cells were concentrated in the western coastal area and the western region of the TBM Range over the central Korean Peninsula. The concentration on the western side of the TBM Range might occur because the storm propagation across the TBM Range was obstructed by the terrain.

In this case, two different MCSs with heavy rainfall occurred successively over the central Korean Peninsula at 1000 and 1800 UTC 26 July. These two MCSs had different characteristics in terms of the initiation, evolution, and movement of the storms. At 1000 UTC, the first MCS was generated in the vicinity of a mesoscale, low-level convergence area, developed rapidly, and sustained with a trough tilted with a mesocyclone, and the induction of RIJ at the midlevel of the storm.

Compared to the first MCS, the initiation of the second MCS at 1800 UTC was not directly related to a mesoscale low-level convergence. The small convective storms coalesced into a large storm cluster and were controlled by the cluster movement. We presumed that the convective storms in the second MCS initiated along the cold outflow boundaries from the preexisting storms in the first MCS. The pattern of movement and the propagation of the storms is a direct factor in flash flooding. In this case, the two MCSs had rather different patterns of storm movement and propagation. The first MCS moved eastward relatively quickly along the environmental winds, and new storms generated on the downstream side of the MCS (forward propagation). The severity of the individual storms in the first MCS was considerable but resulted in small rainfall amounts over the threat region due to the rapid movement. On the other hand, the second MCS had favorable conditions for flash flooding. The number of long-lived storms (≥ 1 h) in the second MCS suddenly increased to 3 times the total number of convective cells in the first MCS. A large storm merged with peripheral storms forming a cluster, and then new storms were continually generated on the upstream side, merging with the cluster (backward propagation). The clusters moved in a rightward direction almost perpendicular to the movement of individual cells and the environmental wind. Later, the clusters stagnated over Chorwon, Yonchon, and the Imjin River basin for longer than 8 h. The long-lived storm was characterized by a widespread low-level easterly inflow, midlevel RIJ, and upper-level divergence. It is likely that the RIJ and vertical wind shear in the storm prolonged the lifetime of the storm and delayed the decay of the storm by downdraft.

Acknowledgments. We thank Major (Dr.) Peter B. Roohr at the Air Force Weather Agency and Major (retired) Kenneth Carey of the Mitretek Systems Inc. for providing WSR-88D level II data and useful comments for this study. This study was supported by the Korea Science and Engineering Foundation through the Advanced Basic Research Laboratory Program and by the Korea Meteorological Administration through the Research Program on Dynamical and Physical Processes and Technology Development of Prediction of Cloud-Scale Heavy Rainfall.

REFERENCES

- Bluestein, H. B., 1993: *Observations and Theory of Weather Systems*. Vol. II, *Synoptic-Dynamic Meteorology in Midlatitudes*, Oxford University Press, 594 pp.
- , and M. H. Jain, 1985: Formation of mesoscale lines of precipitation: Severe squall lines in Oklahoma during the spring. *J. Atmos. Sci.*, **42**, 1711–1732.
- Burgess, D., and P. S. Ray, 1986: Principle of radar. *Mesoscale Meteorology and Forecasting*, P. S. Ray, Ed., Amer. Meteor. Soc., 85–117.
- Byun, H. R., 1995: The pattern classification of the heavy rains and its associated atmospheric circulation. *Int. Workshop on Heavy Rainfall in East Asia*, Seoul, South Korea, Atmospheric and Environmental Research Institute/Seoul National University and Korea Science and Engineering Foundation, 90–101.
- Chappell, C. F., 1986: Quasi-stationary convective events. *Mesoscale Meteorology and Forecasting*, P. S. Ray, Ed., Amer. Meteor. Soc., 289–310.
- Chun, J. K., and M. L. Oh, 1991: Presumption of the horizontal wind and divergence field using a single Doppler radar data (in Korean). *J. Kor. Meteor. Soc.*, **27**, 55–66.
- Doswell, C. A., III, Ed., 2001: *Severe Convective Storms*. Meteor. Monogr., No. 50, Amer. Meteor. Soc., 570 pp.
- ERS, 2004: RAOB version 5.5 user's guide and technical manual. Environmental Research Services, 102 pp.
- Fritsch, J. M., and G. S. Forbes, 2001: Mesoscale convective systems. *Severe Convective Storms*, Meteor. Monogr., No. 50, Amer. Meteor. Soc., 323–357.
- Fulton, R. A., J. P. Breidenbach, D. J. Seo, D. A. Miller, and T. O'Bannon, 1998: The WSR88D rainfall algorithm. *Wea. Forecasting*, **13**, 377–395.
- Funk, T., cited 2004: Heavy convective rainfall forecasting: Parameters, processes, patterns, and rule of thumb. Science and Technology, NWS, Louisville, KY, 38 pp. [Available online at http://www.crh.noaa.gov/lmk/soo/presentations/heavy_rainfall_forecasting.pdf.]
- Houze, R. A., S. A. Rutledge, M. I. Biggerstaff, and B. F. Smull, 1989: Interpretation of Doppler radar displays of midlatitude mesoscale convective systems. *Bull. Amer. Meteor. Soc.*, **70**, 608–619.
- Johnson, J. T., P. L. Mackeen, A. Witt, E. D. Mitchell, G. J. Stumpf, M. D. Elts, and K. W. Thomas, 1998: The Storm Cell Identification and Tracking (SCIT) algorithm: An enhanced WSR-88D algorithm. *Wea. Forecasting*, **13**, 263–276.
- Junker, N. W., R. S. Schnieder, and S. L. Fauver, 1999: A study of heavy rainfall events during the great Midwest flood of 1993. *Wea. Forecasting*, **14**, 701–712.
- KMA, 1996: Annual report (in Korean). Korea Meteorological Administration, 256 pp.
- Lee, D. K., and H. R. Kim, 1995: Numerical simulation of 10 heavy rainfall cases over the Korean Peninsula. *Int. Workshop on Heavy Rainfall in East Asia*, Seoul, South Korea, Atmospheric and Environmental Research Institute/Seoul National University and Korea Science and Engineering Foundation, 114–133.
- , —, and S. Y. Hong, 1998: Heavy rainfall over Korea during 1980–1990. *Kor. J. Atmos. Soc.*, **1**, 32–50.
- Lee, M. S., and D. K. Lee, 2003: An application of a weakly constrained 4DVAR to satellite data assimilation and heavy rainfall simulation. *Mon. Wea. Rev.*, **131**, 2151–2176.
- Lemon, L. R., 1998: The radar “three-body scatter spike”: An operational large-hail signature. *Wea. Forecasting*, **13**, 327–340.
- Lin, Y.-L., S. Chiao, T. A. Wang, M. L. Kaplan, and R. P. Weglarz, 2001: Some common ingredients for heavy orographic rainfall. *Wea. Forecasting*, **16**, 633–660.
- Moteki, Q., H. Uyeda, T. Maesaka, T. Shinoda, M. Yoshizaki, and T. Kato, 2004a: Structure and development of two merged rainbands observed over the East China Sea during X-BAIU-

99. Part I: Meso- β -scale structure and development processes. *J. Meteor. Soc. Japan*, **82**, 19–44.
- , —, —, —, —, and —, 2004b: Structure and development of two merged rainbands observed over the East China Sea during X-BAIU-99. Part II: Meso- α -scale structure and build-up processes of convergence in the Baiu frontal region. *J. Meteor. Soc. Japan*, **82**, 45–65.
- Moller, A. R., 2001: Severe local storms forecasting. *Severe Convective Storms, Meteor. Monogr.*, No. 50, Amer. Meteor. Soc., 433–480.
- NWS, cited 2004: Convective season environmental parameters and indices. Science and Technology, NWS, Louisville, KY. [Available online at <http://www.crh.noaa.gov/lmk/soo/docu/indices.php>.]
- Seo, D.-J., J. Breidenbach, R. Fulton, and D. Miller, 2000: Real-time adjustment of range-dependent biases in WSR-88D rainfall estimates due to nonuniform vertical profiles of reflectivity. *J. Hydrometeor.*, **1**, 222–240.
- Serafin, R., and J. W. Wilson, 2000: Operational weather radar in the United States: Progress and opportunity. *Bull. Amer. Meteor. Soc.*, **81**, 501–518.
- Shinoda, T., and H. Uyeda, 2002: Effective factors in the development of deep convective clouds over the wet region of eastern China during the summer monsoon season. *J. Meteor. Soc. Japan*, **80**, 1395–1414.
- SSAD, 1998: WATADS: Reference guide for version 10.0. Storm Scale Applications Division, National Severe Storms Laboratory, 72 pp. [Available from Storm Scale Applications Division, National Severe Storms Laboratory, 1313 Halley Circle, Norman, OK 73069.]
- Stensrud, D. J., R. L. Gall, and M. K. Nordquist, 1997: Surges over the Gulf of California during the Mexican monsoon. *Mon. Wea. Rev.*, **125**, 417–437.
- Stumpf, G. J., A. Witt, E. D. Mitchell, P. L. Spencer, J. T. Johnson, M. D. Eilts, K. W. Thomas, and D. W. Burgess, 1998: The National Severe Storm Laboratory Mesocyclone Detection Algorithm (MDA) for the WSR-88D. *Wea. Forecasting*, **13**, 304–326.
- Sun, J., and T. Y. Lee, 2002: A numerical study of an intense quasi-stationary convection band over the Korean Peninsula. *J. Meteor. Soc. Japan*, **80**, 1221–1245.
- Takeda, T., and K. Takase, 1980: Radar observation of rainfall system modified by orographic effects. *J. Meteor. Soc. Japan*, **58**, 500–515.
- UCAR, 2002: *Heavy Precipitation and Flash Flooding*. University Corporation for Atmospheric Research–Cooperative Program for Operational Meteorology, Education, and Training, Laser Disk. [Available from COMET, P.O. Box 3000, Boulder, CO 80307-3000.]
- Watanabe, H., and Y. Ogura, 1987: Effects of orographically forced upstream lifting on mesoscale heavy precipitation: A case study. *J. Atmos. Sci.*, **44**, 661–675.
- Wee, T. K., 1999: A cumulus parameterization based on cloud-resolving simulations of mesoscale convective systems (in Korean). Ph.D. thesis, Seoul National University, Seoul, South Korea, 308 pp.
- Weisman, M. L., 1992: The role of convectively generated rear-inflow jets in the evolution of long-lived mesoconvective systems. *J. Atmos. Sci.*, **49**, 1826–1847.
- , and J. B. Klemp, 1984: The structure and classification of numerically simulated convective storms in directionally varying wind shears. *Mon. Wea. Rev.*, **112**, 2479–2498.
- , and —, 1986: Characteristics of isolated convective storms. *Mesoscale Meteorology and Forecasting*, P. S. Ray, Ed., Amer. Meteor. Soc., 341–358.
- Zipser, E. J., 1982: Use of a conceptual model of the life-cycle of mesoscale convective systems to improve very short-range forecasts. *Nowcasting*, K. Browning, Ed., Academic Press, 191–204.